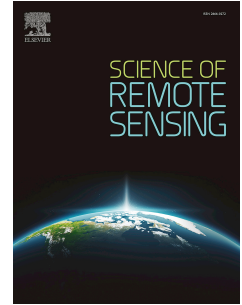


Journal Pre-proof

Spatial downscaling of SMAP radiometer soil moisture using radar data: Application of machine learning to the SMAPEX and SMAPVEX campaigns

Elaheh Ghafari, Jeffrey P. Walker, Liujun Zhu, Andreas Colliander, Alireza Faridhosseini



PII: S2666-0172(24)00006-3

DOI: <https://doi.org/10.1016/j.srs.2024.100122>

Reference: SRS 100122

To appear in: *Science of Remote Sensing*

Received Date: 5 August 2023

Revised Date: 6 February 2024

Accepted Date: 6 February 2024

Please cite this article as: Ghafari, E., Walker, J.P., Zhu, L., Colliander, A., Faridhosseini, A., Spatial downscaling of SMAP radiometer soil moisture using radar data: Application of machine learning to the SMAPEX and SMAPVEX campaigns, *Science of Remote Sensing* (2024), doi: <https://doi.org/10.1016/j.srs.2024.100122>.

This is a PDF file of an article that has undergone enhancements after acceptance, such as the addition of a cover page and metadata, and formatting for readability, but it is not yet the definitive version of record. This version will undergo additional copyediting, typesetting and review before it is published in its final form, but we are providing this version to give early visibility of the article. Please note that, during the production process, errors may be discovered which could affect the content, and all legal disclaimers that apply to the journal pertain.

© 2024 Published by Elsevier B.V.

1 **Spatial downscaling of SMAP radiometer soil moisture using radar data: Application of**
2 **machine learning to the SMAPE_x and SMAPVEX campaigns**

3 Authors: Elaheh Ghafari^{a*}, Jeffrey P. Walker^b, Liujun Zhu^{b,c}, Andreas Colliander^d, Alireza
4 Faridhosseini^a

5 ^a *Department of Water Engineering, Ferdowsi University of Mashhad, Mashhad, Iran*

6 ^b *Department of Civil Engineering, Monash University, Melbourne, Australia*

7 ^c *Yangtze Institute for Conservation and Development, Hohai University, Nanjing, 210024,*
8 *China*

9 ^d *Jet Propulsion Laboratory, NASA, California Institute of Technology, Pasadena, CA 91109,*
10 *USA*

11

12 Submitted to: Science of Remote Sensing

13 Submitted Date: 5 August 2023

14 *Corresponding Author: Elaheh Ghafari (Email: ghafarielaheh84@gmail.com)

15 Email addresses: ghafarielaheh84@gmail.com (E. Ghafari), Jeff.Walker@monash.edu (J.P.

16 Walker), Liujun.zhu@hhu.edu.cn (L. Zhu), andreas.colliander@jpl.nasa.gov (A. Colliander),

17 farid-h@um.ac.ir (A. Faridhosseini)

18 ABSTRACT:

19 This study developed a random forest approach for downscaling the coarse-resolution (36 km)
20 soil moisture measured by The National Aeronautics and Space Administration (NASA) Soil
21 Moisture Active Passive (SMAP) mission to 1 km spatial resolution, utilizing airborne
22 remotely sensed data (radar backscatter and radiometer retrieved soil moisture), vegetation
23 characteristics (normalized difference vegetation index), soil properties, topography, and
24 ground soil moisture measurements from before the launch of SMAP for training a random
25 forest model. The 36 km SMAP soil moisture product was then downscaled by the trained
26 model to 1 km resolution using the information from SMAP. The downscaled soil moisture
27 was evaluated using airborne retrieved soil moisture observations and ground soil moisture
28 measurements. Considering the airborne retrieved soil moisture as a reference, the results
29 demonstrated that the proposed random forest model could downscale the SMAP radiometer
30 product to 1 km resolution with a correlation coefficient of 0.97, unbiased Root Mean Square
31 Error of $0.048 \text{ m}^3 \cdot \text{m}^{-3}$ and bias of $0.016 \text{ m}^3 \cdot \text{m}^{-3}$. Accordingly, the downscaled soil moisture
32 captured the spatial and temporal heterogeneity and demonstrated the potential of the proposed
33 machine learning model for soil moisture downscaling.

34 Keywords: Machine learning, Downscaling, Soil moisture, SMAP, Random forest model,
35 SMAPE_x, SMAPVEX

36 Highlights:

- 37 • A random forest machine learning model was developed to downscale the SMAP
38 radiometer soil moisture.
- 39 • The random forest model was trained using active-passive microwave, landscape, and
40 vegetation data.
- 41 • Airborne pre- / post-launch data was used to train and subsequently validate the
42 downscaling model.
- 43 • Training to soil moisture data over 1 km grid cells decreased the training scale-
44 mismatch.
- 45 • Assessment of variables showed the importance of horizontal polarised backscatter and
46 terrain slope.

47

48

49

50

51 **1. Introduction**

52 Soil moisture is an important variable in the hydrology, climatology, and agricultural
53 sciences, as it is an essential factor in controlling the global water, energy and carbon cycles,
54 linking land and atmospheric parameters (Seneviratne et al. 2010). Over the last decade, the
55 possibility of global soil moisture monitoring has been made possible by the advent of remote
56 sensing techniques (Entekhabi et al. 2010; Kerr et al. 2012). Accordingly, L-band passive
57 microwave at 1.41 GHz frequency has been adopted as the preferred approach due to its ability
58 to monitor data under all weather conditions, the direct relationship between passive
59 microwave observation and soil moisture, and the low sensitivity to atmospheric effects,
60 surface roughness and vegetation (Gao et al. 2022; Schmugge et al. 1986). Therefore, L-band
61 satellites such as Soil Moisture and Ocean and Salinity (SMOS) mission were launched to
62 provide global soil moisture maps (Barre et al. 2008). However, the low spatial resolution of
63 passive microwave sensors is a major limitation to many applications. Consequently,
64 investigations demonstrated that combining active (radar) and passive (radiometer) microwave
65 observations can enhance the resolution by combining their respective advantages, including the
66 high accuracy of passive observations with the fine spatial resolution of active observations
67 (Das et al. 2011; Entekhabi et al. 2010). This method has been termed as active passive.

68 On the 31st January 2015, the Soil Moisture Active Passive (SMAP) satellite was launched
69 by the National Aeronautics and Space Administration (NASA), to provide global soil moisture
70 maps of the top 5 cm soil surface with a temporal resolution of 2 to 3 days and spatial resolution
71 of 9 km (Entekhabi et al. 2014). This was to be achieved by combining 1.26 GHz radar
72 backscatter (σ) at 3 km resolution and 1.41 GHz radiometer brightness temperature (T_b) at 36
73 km resolution, with the aim to provide a soil moisture accuracy better than $0.04 \text{ m}^3 \cdot \text{m}^{-3}$ (Chan
74 et al. 2016). However, the SMAP radar instrument stopped working in July 2015, leaving only
75 the radiometer observations measured by SMAP. Consequently, investigations have focused

76 on generating a high resolution soil moisture product by combining the SMAP radiometer with
77 other radar observations, such as those from the Copernicus Sentinel-1 C-band radar (Das et
78 al. 2019; Ghafari et al. 2020). Moreover, the data that was collected during the period the radar
79 was working has provided an important experimental data set for developing and testing a
80 variety of downscaled SMAP products using a range of data and algorithms (Colliander et al.
81 2017a; Sabaghy et al. 2018; Wu et al. 2016; Wu et al. 2015).

82 In recent years, several alternate methods have emerged for downscaling the coarse
83 resolution SMAP and SMOS soil moisture products (Das et al. 2011; Kim and Zyl 2009; Merlin
84 et al. 2012; Narayan et al. 2006; Piles et al. 2011). Among these approaches are machine
85 learning methods, whereby optical and thermal observations, along with static
86 geomorphological data at high spatial resolution are usually used as the covariates to downscale
87 the passive microwave soil moisture product (Fang and Shen 2020; Karthikeyan and Mishra
88 2021; Long et al. 2019). However, investigations on utilizing radar observations as a covariate
89 for machine learning methods has been limited (Mao et al. 2019; Zhu et al. 2021). Several
90 investigations have shown that among all the machine learning methods used for downscaling
91 satellite-based products, being either the derived soil moisture or the observed brightness
92 temperature, the random forest algorithm has shown the greater performance, as it is a more
93 flexible model due to randomization and use of an ensemble approach (Abbaszadeh et al. 2019;
94 Hu et al. 2020; Lei et al. 2022; Mao et al. 2022; Rao et al. 2022; Zhao et al. 2018).

95 To ensure a robust satellite downscaling algorithm, this study used completely independent
96 pre- and post-launch information for the training and testing phases of the machine learning
97 model development, respectively. Moreover, a random forest model was developed, based on
98 vegetation characteristics, topography, properties of the top 5 cm soil layer, and the soil
99 moisture datasets available at only focus monitoring sites, for downscaling the coarse
100 resolution SMAP passive soil moisture (36 km) to fine spatial resolution (1 km). This was

101 achieved utilizing the third Soil Moisture Active Passive Experiment (SMAPEX-3) and Soil
102 Moisture Active Passive Validation Experiment 2012 (SMAPVEX-12) campaigns. Previous
103 studies commonly used the 36 km SMAP grid cell soil moisture as the 1 km soil moisture input
104 variable to construct the downscaling model (Abbaszadeh et al. 2019; Hu et al. 2020; Rao et
105 al. 2022). Consequently, one of the novelties of this paper is utilizing soil moisture at the
106 downscaling target resolution of 1 km as input to the training phase of the machine learning,
107 as provided by pre-launch campaigns, instead of the coarse passive SMAP soil moisture.
108 Furthermore, most machine learning approaches to date have validated the output at just a few
109 in situ points (Abowarda et al. 2021; Lei et al. 2022; Long et al. 2019). However, this study
110 used the microwave soil moisture data retrieved from airborne passive observations across
111 several SMAP pixels at 1 km resolution for validation, along with all available ground soil
112 moisture measurements, to ensure the accuracy of the achieved spatial patterns in soil moisture.

113 **2. Study area**

114 Two field experiment sites were selected as the study areas due to their large-scale airborne
115 and ground campaigns; the Soil Moisture Active Passive Experiments (SMAPEX) field
116 campaigns carried out in south-eastern Australia, and the Soil Moisture Active Passive
117 Validation Experiment 2012 (SMAPVEX-12) field campaign conducted in south central
118 Manitoba, Canada. The extensive pre-launch data make these very suitable study areas for the
119 purpose of this research. Combining the data from both campaigns provided a sufficiently large
120 sample size for training the algorithm. Furthermore, these sites present complementary soil
121 characteristics, weather status and vegetation coverage, thus providing a wide range of
122 conditions. More detailed descriptions about the field campaigns follow.

123 **2.1. Soil Moisture Active Passive Experiment (SMAPEX) campaigns**

124 Five airborne field campaigns were undertaken over the period from 2010 to 2015 in south-
125 eastern Australia, known as the Soil Moisture Active Passive Experiments (SMAPEX)
126 (Panciera et al. 2014; Ye et al. 2020). These were conducted in the Yanco SMAP validation
127 area in the Murrumbidgee River catchment (Fig. 1). SMAPEX-1 to SMAPEX-3 were
128 undertaken before the SMAP launch, while SMAPEX-4 and SMAPEX-5 were conducted post-
129 launch. These campaigns were designed with the basic target of developing the soil moisture
130 algorithms for SMAP products at pre-launch, and for calibration and validation of SMAP
131 observations and downscaled soil moisture at post-launch. Accordingly, during the SMAPEX
132 campaigns, airborne passive and active observations were made similar to the SMAP
133 observations (Wu et al. 2015), and the ground soil moisture and several kinds of ancillary data
134 were collected coincident with SMAP overpasses. The third to fifth SMAPEX campaigns,
135 which were utilized in this research for developing and then testing the machine learning
136 downscaling model, were conducted in the austral spring (5th to 23rd September, 2011), autumn
137 (30th April to 23rd May, 2015), and spring (6th to 28th September, 2015), respectively. These
138 campaigns provided valuable datasets for developing the SMAP downscaling algorithm under
139 Australian soil and vegetation conditions (Panciera et al. 2014). More details about the
140 SMAPEX datasets are in the workplan reports available at <https://www.smapex.monash.edu>,
141 so only a brief outline of the information is presented here.

142 The dataset from the SMAPEX-3 campaign included six focus areas, being a 3 km × 3 km
143 grid cell for each, corresponding to the EASE-2 SMAP grid cells across the SMAP radiometer
144 pixel. These were used for constructing the downscaling model during the training phase of
145 establishing the machine learning algorithm (Fig. 1). It is notable that only data from the third
146 SMAPEX campaign was used at this step. The datasets during the SMAPEX-4 and SMAPEX-5
147 experiments, covering approximately six coarse resolution SMAP grid cells over the SMAP
148 validation flight area (Fig. 1), were utilized for validating the algorithm. The variability in soil

149 and vegetation conditions, the availability of the soil moisture dataset measured based on the
150 ground experiments, and the availability of the required airborne and satellite data make these
151 selected areas appropriate for research on microwave retrieval of soil moisture from satellites.
152 The selected study site is located in a semi-arid area with flat topography. The six selected
153 ground-sampling sites are called YA4, YA7, YB5, YB7, YE and YF. The land use of the sites
154 is irrigated cropping (90%) and grazing (10%) for YA4 and YA7, irrigated cropping (85%) and
155 grazing (15%) for YF, and entirely grazing for YB5, YB7 and YE. Therefore, the two main
156 land cover types were cropping and grazing. The soil textures are categorized as clay loam for
157 YA4 and YA7, silty clay loam for YE, and loam for YB5, YB7 and YF. The soil texture was
158 obtained from gravimetric samples used to extract the soil particle distribution (Monerris et al.
159 2011) and the CSIRO Digital Atlas of Australian Soils (1991).

160 The SMAPEX-3 campaign took place in the austral spring, with moderate rainfall in the
161 first half of the period resulting in a soil moisture dry down, and winter crops in their intensive
162 growth periods. More descriptions of SMAPEX-3 are available in Panciera et al. (2014). The
163 SMAPEX-4 campaign took place in the austral autumn. During this experiment, crop areas with
164 dry or burned corn stubble or rice straw residual from harvest were dominant, while some crop
165 areas had been ploughed for seeding. Consequently, the surface roughness was high due to the
166 deep furrows in the ploughed and harvested areas, while the grazing area was covered by short
167 grass. The range in soil moisture conditions was around $0.1 \text{ m}^3 \cdot \text{m}^{-3}$ and the average vegetation
168 water content was approximately $0.1 \text{ kg} \cdot \text{m}^{-2}$. Before the campaign began, several heavy rainfall
169 events occurred which made for heterogenous soil conditions during the dry down period in
170 the selected area. Two medium rainfall events also occurred during the campaign, providing
171 further heterogeneity to the soil water content distributions (Ye et al. 2020). The last campaign,
172 SMAPEX-5, took place in the austral spring when the vegetation had high growth rates, with
173 VWC up to approximately $2 \text{ kg} \cdot \text{m}^{-2}$. Heavy rainfall occurred before the campaign providing

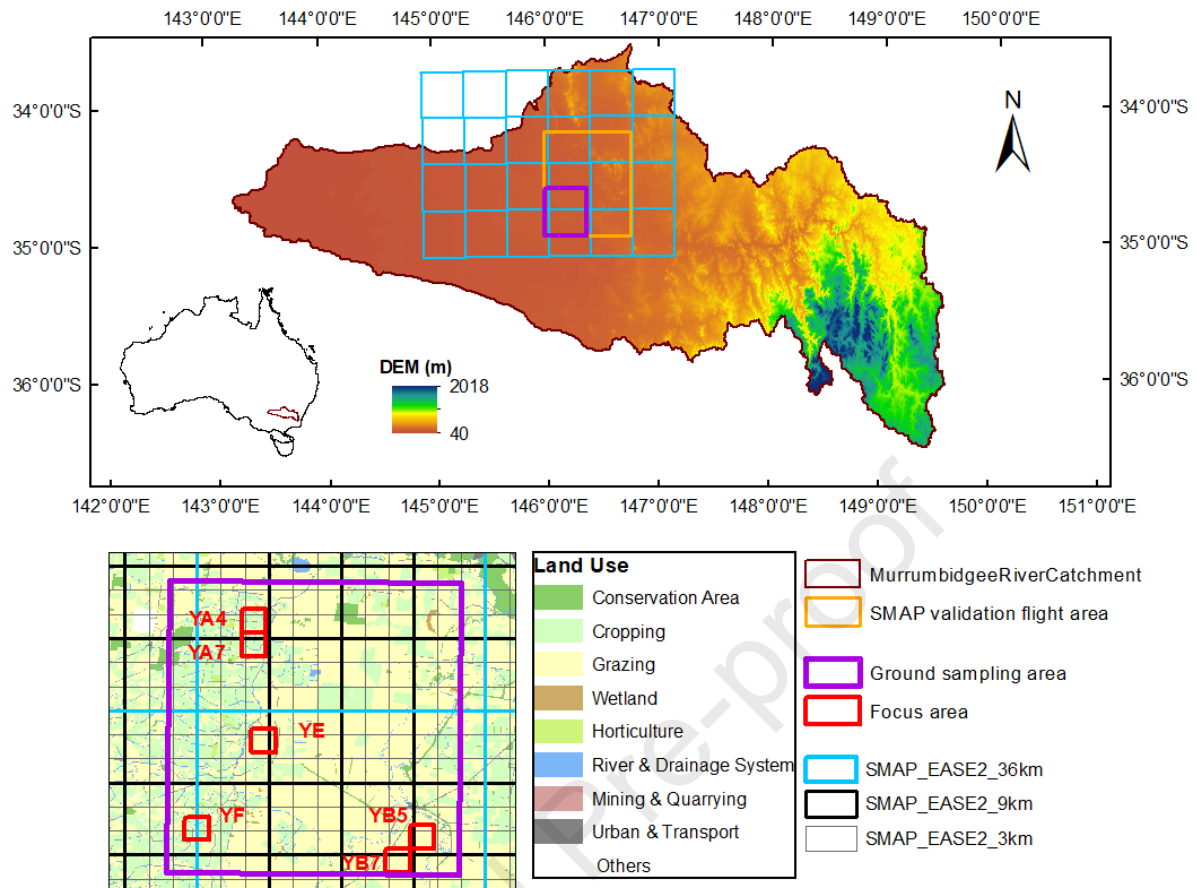


Fig. 1. The SMAPEX study site in the Murrumbidgee River catchment in south-eastern of Australia with the Digital Elevation Model (DEM), and the six focus areas used for ground sampling, together with the SMAP grid cells overlain with the land use map.

174 heterogeneity in soil moisture conditions along with a dry down situation. The most vegetated
 175 area during this campaign was the irrigated and dryland cropping, followed by grazing land
 176 (Ye et al. 2020).

177 **2.2. The Soil Moisture Active Passive Validation Experiment 2012 (SMAPVEX-12)** 178 **campaign**

179 The SMAPVEX-12 field campaign was conducted at the pre-launch stage of SMAP to
 180 assist SMAP algorithm development. The campaign was conducted at the Canadian Red River
 181 Watershed in south central Manitoba, Canada (Fig. 2), mostly covered by agricultural and some

182 forest areas (McNairn et al. 2015). The period of the SMAPVEX-12 experiment was from June
183 17th to July 19th, 2012, with the intent of collecting active and passive airborne observations
184 together with ground soil moisture measurements and ancillary datasets. The size of the site
185 was 12.8 km × 70 km, capturing forest and agricultural areas (Fig. 2). The soil texture varied
186 from heavy clays to fine loamy sand through the east to west of the study area, leading to
187 substantial soil moisture gradients over short distances. The site is predominately flat with a
188 maximum slope of 2%. Ground soil moisture data were acquired by permanent soil moisture
189 stations installed by Agriculture and Agri-food Canada, manual sampling teams, and temporary
190 sites installed by the United States Department of Agriculture (USDA).

191 As shown in Fig. 2, the selected site was dominated by a mix of agricultural area, mostly
192 including cereals and oil seeds. Overall, 67% of the site was covered by crops and
193 approximately 15% by grassland and pasture. Seeding was undertaken in April/May and
194 harvesting in August/September. Fifty-five agricultural fields of at least 800 m × 800 m in size
195 were monitored throughout the SMAPVEX-12 campaign, collecting ground soil moisture
196 measurements as shown in Fig. 2. As both cropland and grassland data were available, the
197 SMAPVEX-12 campaign provided useful information to complement the SMAPEX campaign
198 dataset for downscaling the SMAP soil moisture utilizing the machine learning algorithm.
199 Further details about the campaign are available in McNairn et al. (2015), with the SMAPVEX-
200 12 datasets accessible at <https://nsidc.org/data/smap/validation-data>.

201 **3. Data**

202 **3.1. SMAP radiometer soil moisture product**

203 The SMAP satellite provides global scale soil moisture maps of the top 5 cm, with an
204 *ubRMSE* of less than 0.04 m³.m⁻³ (Bindlish et al. 2016). This research utilized a machine
205 learning approach for downscaling the SMAP radiometer-based soil moisture product. The

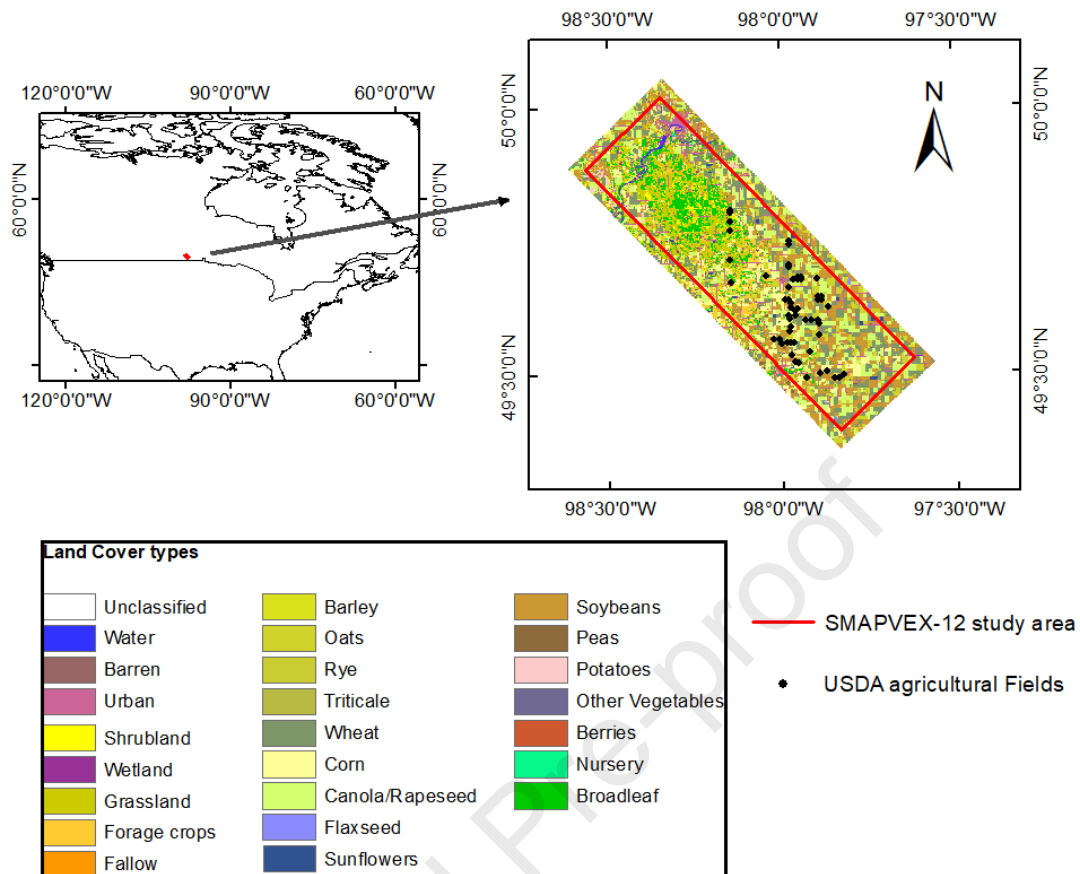


Fig. 2. Overview of the SMAPVEX-12 study site located at the Red River watershed in south-central Manitoba in Canada overlain with the land cover types and the location of USDA agricultural fields.

206 descending overpass of the SMAP L3 radiometer 36 km EASE-grid soil moisture product
 207 version 8 (L3_SM_P) was selected for this purpose (O'Neill et al. 2021). This product is
 208 available at <https://nsidc.org/data/SPL3SMP/versions/8>.

209 3.2. Active and passive airborne datasets

210 The airborne instruments used in the SMAPEX campaigns included the 1.41 GHz
 211 Polarimetric L-Band Multibeam Radiometer (PLMR) and the 1.26 GHz Polarimetric L-Band
 212 Imaging Synthetic Aperture Radar (PLIS), which provided the L-band passive (brightness
 213 temperature) and active (backscatter) microwave observations. Overall, there are nine flight
 214 dates from SMAPEX-3 (5th, 7th, 10th, 13th, 15th, 18th, 19th, 21st and 23rd September, 2011), six

215 flight dates from SMAPEX-4 (2nd, 5th, 10th, 11th, 19th and 21st May, 2015) and eight flight dates
216 from SMAPEX-5 (8th, 10th, 13th, 16th, 18th, 21st, 23rd and 26th September, 2015) covering several
217 3 dB SMAP radiometer footprints. Notably, SMAPEX-4 data was coincident with both SMAP
218 radiometer and radar observations.

219 The passive airborne radiometer brightness temperature data for SMAPEX experiments was
220 collected by the PLMR instrument with 1 km spatial resolution at horizontal and vertical (h
221 and v) polarizations and nominal incidence angles of 17°, 21.5° and 38.5°. An accuracy of
222 around ± 1.4 K was obtained for the calibration of PLMR brightness temperature at vertical
223 and horizontal polarization, and an accuracy of about ± 1.5 K for thermal correction of the
224 calibrated dataset was achieved during the SMAPEX campaigns (Ye et al. 2020). The PLMR
225 brightness temperature observations were angle normalized from their original angles to the
226 reference incidence angle of SMAP ($\sim 40^\circ$) utilizing a cumulative distribution function
227 approach (Ye et al. 2015). An accuracy of about ± 2.4 K was achieved for angle normalization
228 of the PLMR brightness temperature (Wu et al. 2015). As the SMAP soil moisture data did not
229 exist for the training phase, due to being in the pre-launch period, the SMAPEX-3 airborne
230 retrieved soil moisture at 1 km spatial resolution (Ye et al. 2020) was averaged to 36 km
231 resolution to simulate the SMAP derived soil moisture data to train the machine learning
232 algorithm. Additionally, the derived soil moisture observations from SMAPEX-4 and
233 SMAPEX-5 PLMR brightness temperature at 1 km spatial resolution over the entire SMAP
234 validation flight area (Fig. 1) were used in the testing phase of the machine learning algorithm
235 development, for the purpose of evaluating the downscaling algorithm results. During the
236 SMAPEX experiments, the airborne radar backscatter datasets were measured by the PLIS
237 instrument at hh , hv , vh and vv polarizations, high temporal resolution and 10 m spatial scale
238 (Ghafari et al. 2020; Zhu et al. 2018) with an incidence angle between 15° to 45°. The PLIS
239 instrument provided complete coverage over the study area during SMAPEX-3, but with small

240 gaps across the SMAPEX-4 and 5 campaigns due to the flight design. However, previous
241 investigations on the PLIS coverage gaps demonstrated that there was a nonsignificant effect
242 on the accuracy of the PLIS backscatter when processed to 3 km resolution for use in
243 downscaling (Ghafari et al. 2020). Before using the PLIS observations in the machine learning
244 technique, the data was calibrated, georeferenced, and normalized for the incidence angle, with
245 an accuracy of 0.58 dB achieved for calibration (Zhu et al. 2018). To normalize the PLIS
246 incidence angle to that of SMAP (40°), the method utilized for angle normalization of the
247 PLMR observations was performed (Ye et al. 2015). An accuracy of 0.8 dB was achieved for
248 the angle normalized backscatter data at 1 km resolution (Wu et al. 2015). Finally, the PLIS
249 backscatter data was aggregated by linear averaging from the original grid cell (10 m) to the
250 required resolution (1 km). In this study, the vertical and horizontal co-polarized and cross-
251 polarized PLIS backscatter (σ_{vv} , σ_{hh} and σ_{xpol}) were used.

252 The airborne instrument of the SMAPVEX-12 campaign is called the Passive Active L-
253 band Sensor (PALS), providing L-band radiometer brightness temperature with both vertical
254 and horizontal polarization at 1.41 GHz frequency, and L-band radar backscatter with hh , hv ,
255 vh and vv polarizations at 1.26 GHz frequency. The PALS instrument was mounted to provide
256 a single beam with a 40° incidence angle looking to the rear of the aircraft (McNairn et al.
257 2015). Sixteen flight dates of SMAPVEX-12 (7th, 12th, 15th, 17th, 22nd, 25th, 27th and 29th June,
258 and 3rd, 5th, 8th, 10th, 13th, 14th, 17th and 19th July, 2012) provided active and passive airborne
259 measurements for the machine learning algorithm training over the SMAPVEX-12 area. In this
260 research, the calibrated co-polarized and cross-polarized PALS backscatter observations (σ_{vv} ,
261 σ_{hh} and σ_{xpol}), Version 1 (SV12PLBK) (Colliander 2014) measured over SMAPVEX-12
262 agricultural sampling fields (nominal size of 800 m × 800 m) were resampled through a linear
263 averaging approach to provide the 1 km resolution radar observations, while the retrieved soil
264 moisture data, Version 1 (SV12PLSM) achieved from PALS brightness temperature

265 observations (Colliander 2017; Colliander et al. 2016) at 1 km spatial resolution was utilized
266 to simulate the 36 km SMAP soil moisture. The SMAPVEX data was only used in the training
267 step of developing the machine learning based downscaling algorithm. More description about
268 the PALS instrument and its radar and radiometer calibration methodologies are available in
269 McNairn et al. (2015).

270 **3.3. MODIS Normalized Difference Vegetation Index (NDVI)**

271 Machine learning methods are able to integrate various data sources. Utilizing vegetation
272 index parameters in the satellite soil moisture downscaling methods has been one of the widely
273 accepted approaches over the past decade (Fang and Lakshmi 2014; Merlin et al. 2008; Piles
274 et al. 2011). The MODerate resolution Imaging Spectroradiometer (MODIS) is a multispectral
275 instrument of the NASA Earth Observing System, consisting of Aqua and Terra satellites
276 which measure the visible, near infrared, and thermal infrared signatures at 36 spectral bands
277 every 1 to 2 days. In this study the daytime overpass of Terra, being most consistent with the
278 SMAP overpass, was selected to extract the NDVI variable. The selected MODIS product was
279 the version-061 daily surface spectral reflectance (MOD09GA) at 1 km spatial resolution,
280 available at <https://e4ftl01.cr.usgs.gov/MOLT/>. The reflectance product is available at 500 m
281 spatial resolution. However, for consistency with the microwave data it was resampled to 1 km
282 resolution before calculating NDVI.

283 **3.4. Soil texture data**

284 Soil texture, including clay, silt and sand content, is one of the basic parameters affecting
285 the soil moisture values, through its influence on the rate of water infiltration, soil moisture
286 storage and soil drainage characteristics. Accordingly, several studies have shown that
287 information on soil texture can be one of the important sources in downscaling soil moisture
288 using machine learning (Abbaszadeh et al. 2019; Karthikeyan and Mishra 2021).

289 In this study, the machine learning algorithm utilized the information on soil texture (%
290 clay, % silt, and % sand). The soil texture of the SMAPEX ground sampling site is clay loam
291 (31% clay, 48% silt and 20% sand) for YA4 and YA7, silty clay loam (39% clay, 43% silt and
292 17% sand) for YE, and loam (23% clay, 47% silt and 29% sand) for YB5, YB7 and YF. The
293 SMAPEX ground sampling soil texture data values, and also the soil texture information over
294 the SMAP validation flight area (Fig. 1), were obtained from gravimetric experiments that
295 extracted soil particle size distribution and the CSIRO Digital Atlas of Australian Soils (1991).
296 The soil texture information for SMAPVEX-12 was extracted from soil texture data collected
297 by coring devices over each agricultural field as part of the campaign. The soil texture types
298 varied over this selected area including sand (7% clay, 4% silt and 89% sand), loamy sand (6%
299 clay, 6% silt and 88% sand), sandy clay loam (34% clay, 14% silt and 51% sand), sandy loam
300 (16% clay, 9% silt and 75% sand), silty clay loam (40% clay, 56% silt and 4% sand), clay (56%
301 clay, 30% silt and 14% sand), heavy clay (67% clay, 29% silt and 4% sand), clay loam (38%
302 clay, 19% silt and 43% sand) and silty clay (54% clay, 40% silt and 6% sand). This dataset is
303 accessible at <https://nsidc.org/data/smap/validation-data> (Bullock et al. 2014).

304 3.5. Geographic data

305 Soil moisture conditions, especially in the surface layers, are affected by topographic data
306 (Crow et al. 2012). As elevation, terrain slope and aspect have been found to be the important
307 topographic parameters in soil moisture downscaling studies (Mascaro et al. 2011; Wilson et
308 al. 2005), these features were selected for use in the machine learning model developed here to
309 downscale the SMAP soil moisture. The topography of the Murrumbidgee River catchment
310 changes from 50 m to 2000 m (Fig. 1), however, based on the 250 m topography information
311 from the Geoscience Australia Digital Elevation Model (DEM), the elevation at 1 km spatial
312 resolution for the SMAPEX study area only changed from 100 m to 400 m throughout the
313 SMAP validation flight area. The terrain slope and aspect values were derived from DEM

314 information of the SMAP validation flight area, and changed from 0° to 12° and from -1° to
315 360° respectively at 1 km resolution. The DEM product obtained from the ASTER Global-
316 DEM project (<https://asterweb.jpl.nasa.gov/gdem.asp>) has been used for SMAPVEX, having a
317 30 m spatial resolution with a vertical accuracy of 7 m to 14 m. Based on the data extracted
318 from ASTER, the mean elevations at the USDA agricultural fields varied from 237 m to 276
319 m when averaged to 1 km resolution, while the terrain slope and aspect values changed from
320 3° to 7.8° and from 127.2° to 215.1°.

321 **3.6. Ground soil moisture observations**

322 Each of the SMAPEX campaigns included six focus areas (3 km × 3 km) aligned with the
323 SMAP radar grid cells, with dense soil moisture cluster monitoring stations to monitor soil
324 moisture, along with intensive spatial ground sampling (Fig. 1). During the campaigns,
325 intensive soil moisture values were monitored over the 0-5 cm depth concurrent with airborne
326 overpasses at the focus areas using the Hydraprobe Data Acquisition System (HDAS) (Merlin
327 et al. 2007). The soil moisture information was recorded on a 250 m × 250 m grid over each
328 SMAPEX focus area. Three soil moisture values were measured at each ground sample point
329 within a radius of one meter to consider soil moisture variations, reducing the impact of errors
330 in measuring the data. For use in this study, these soil moisture values were aggregated through
331 linear averaging within each 1 km grid, being the target spatial resolution.

332 The selected ground soil moisture of the SMAPVEX-12 experiments for this research was
333 from the temporary soil moisture sensors installed by the United States Department of
334 Agriculture (USDA). As mentioned earlier, there were 55 measurement sites known as
335 agricultural fields (Fig. 2). Soil moisture values during the SMAPVEX-12 experiments varied
336 spatially due to variations in soil texture, the topography of the area, and differences in field
337 irrigation management. To provide valid average soil moisture measurements, sixteen

338 sampling points with three replicates at each point were selected for every agricultural field
339 (mostly 800 m × 800 m fields representing about 1 km spatial resolution) to measure ground
340 soil moisture over the 0-5 cm depth. Replication was utilized to decrease the error resulting
341 from spatial variability in soil properties. The average soil moisture data at each agricultural
342 field was considered as the 1 km ground reference value. The soil moisture was measured using
343 a Stevens Water Hydra Probe (McNairn et al. 2015). The information for the selected datasets
344 is presented in Table 1.

345 **4. Methodology**

346 **4.1. Summary of the Random Forest technique**

347 Random forest is a machine learning method that functions as an ensemble multiple
348 decision tree model (Breiman 1996, 2001). Importantly, the overfit situation may easily occur
349 in the training stage with this approach, leading to poor performance during the testing phase.
350 To overcome this problem, the random forest model makes several decision trees that work
351 individually at the training stage, with the output data achieved by calculating the average
352 prediction of those trees. Accordingly, the input features are divided by the random forest
353 algorithm into several regression trees, so that each tree is produced through a bootstrap sample
354 providing its own prediction value. Overall, the reduction in generalization error occurs due to
355 the combination of results from several decision trees (Breiman 2001). Based on previous
356 research, random forest is the most appropriate machine learning approach for regression and
357 classification problems, such as downscaling of satellite products like soil moisture (He et al.
358 2016; Long et al. 2019; Mao et al. 2022), as it makes the decision trees using the adaptive,
359 randomized and independent features for the relation between input and output variables (Amit
360 and Geman 1997; Breiman 2001).

Table 1. Characteristics of the datasets utilized in the machine learning approach.

| Data set | Details | Source | Spatial resolution | Temporal resolution | Time series / Dates |
|--|---|--|---------------------------------------|---------------------|--|
| SMAP Level 3 soil moisture | Version 8, SMAP radiometer soil moisture product | NSIDC | 36 km | 2-3 days | May, 2015 (six dates) September, 2015 (eight dates) |
| PLMR soil moisture | Airborne soil moisture data from SMAPEX-3, SMAPEX-4 and SMAPEX-5 experiments | smapex.monash.edu | 1 km | Daily | September, 2011 (nine dates) May, 2015 (six dates) September, 2015 (eight dates) |
| PLIS backscatter | Active airborne backscatter data from SMAPEX-3, SMAPEX-4 and SMAPEX-5 experiments | smapex.monash.edu | 10 m (resampled to 1 km) | Daily | September, 2011 (nine dates) May, 2015 (six dates) September, 2015 (eight dates) |
| PALS soil moisture | Airborne soil moisture data from SMAPVEX-12 experiment | NSIDC | 1500 m (resampled to 1 km) | Daily | June, 2012 (eight dates) July, 2012 (eight dates) |
| PALS backscatter | Active airborne backscatter data from SMAPVEX-12 experiment | NSIDC | 500 m, and 1500 m (resampled to 1 km) | Daily | June, 2012 (eight dates) July, 2012 (eight dates) |
| Normalized Difference Vegetation Index (NDVI) | Extracted from MODIS MOD09GA – version 061 | NASA LP DAAC | 1 km | Daily | September, 2011 (nine dates) June, 2012 (eight dates) July, 2012 (eight dates) May, 2015 (six dates) September, 2015 (eight dates) |
| Soil Texture | Variables (% Clay, Silt, Sand) | CSIRO, and SMAPVEX-12 field surveys | 1 km | Static | September, 2011 (nine dates) June, 2012 (eight dates) July, 2012 (eight dates) May, 2015 (six dates) September, 2015 (eight dates) |
| Terrain features | Digital Elevation Model (DEM), Terrain slope and Aspect | Geoscience Australia, and ASTER Global-DEM project | 1 km | Static | September, 2011 (nine dates) June, 2012 (eight dates) July, 2012 (eight dates) May, 2015 (six dates) September, 2015 (eight dates) |
| Ground soil moisture | Focus areas of SMAPEX, and USDA agricultural fields of SMAPVEX-12 | smapex.monash.edu, and NSIDC | Resampled to 1 km | Daily | September, 2011 (nine dates) June, 2012 (eight dates) July, 2012 (eight dates) May, 2015 (six dates) September, 2015 (eight dates) |

361 4.2. Soil moisture downscaling method

362 The target of this research was to develop a random forest algorithm that leads to soil
 363 moisture at finer resolutions (i.e., 1 km), utilizing datasets sourced from before and after the

364 SMAP launch. The basic idea for the approach is to construct a transfer function between
 365 different input variables and the soil moisture output variable using:

$$SM_d = f(C) + \varepsilon, \quad (1)$$

$$C = (c_1, c_2, c_3, \dots, c_N), \quad (2)$$

366 where the SM_d is the downscaled surface soil moisture, ε is the model estimation error, and c_i
 367 demonstrates the individual input variables, including co-polarized and cross-polarized
 368 backscatter (σ_{vv} , σ_{hh} and σ_{xpol}), geographic data (elevation, terrain slope and aspect), soil texture
 369 (% clay, % silt, and % sand), airborne radiometer-based soil moisture and NDVI, and N is the
 370 dimension of input predictors ($N = 11$ in this study).

371 The training of the random forest algorithm used 11 input variables that are at or resampled
 372 to the resolution of 1 km to downscale the SMAP radiometer soil moisture product (L3_SM_P).
 373 These included retrieved soil moisture data from airborne radiometer measurements at 1 km
 374 resolution aggregated to 36 km and radar backscatter in co-polarized and cross-polarized
 375 channels (σ_{vv} , σ_{hh} and σ_{xpol}) aggregated to 1 km, NDVI as being representative of the vegetation
 376 dynamics, soil texture, and geographic data including the Digital Elevation Model (DEM),
 377 derived terrain slope and aspect (Table 1). These parameters have shown a strong relationship
 378 with the temporal dynamics and spatial heterogeneity of soil moisture (Abbaszadeh et al. 2019;
 379 Abowarda et al. 2021; Zhu et al. 2020). As the training phase of the random forest algorithm
 380 needs a source of soil moisture data as the output response variable, the 1 km ground soil
 381 moisture datasets were utilized for this purpose. While the 1 km resolution radiometer
 382 observations could also have been used to aid in the training, this was not done in this instance.
 383 It is notable that over the SMAPEX-3 and SMAPVEX-12 experiments, the ground soil moisture
 384 datasets were only measured at the focus areas (size of $3 \text{ km} \times 3 \text{ km}$ each as shown in Fig. 1)
 385 and at the agricultural fields (size of $800 \text{ m} \times 800 \text{ m}$ each as shown in Fig. 2), respectively.

386 Moreover, the SMAP radar backscatter data from the active passive product
387 (SMAP_L2_SM_AP) resampled to 1 km resolution were used rather than the PLIS backscatter
388 during the SMAPEX-4 campaign.

389 The dataset was split into two groups: i) the data collected before the SMAP launch to train
390 the random forest model, and ii) the data collected after the SMAP launch, unseen by the
391 random forest model, and thus used at the validation phase to verify the resultant downscaling
392 model. Therefore, to investigate the main objective of this study, the data collected during
393 SMAPEX-3 and SMAPVEX-12 (in the years 2011 and 2012, respectively) were used for the
394 training phase of the model, and the data collected during SMAPEX-4 and SMAPEX-5 (in the
395 year 2015) were used for the testing phase. Because the training phase was before the SMAP
396 launch, the radiometer derived soil moisture from SMAPEX-3 and SMAPVEX-12 at 1 km
397 resolution was aggregated to 36 km and used as the input soil moisture data in place of the
398 SMAP 36 km soil moisture during training. In contrast, the SMAP 36 km radiometer soil
399 moisture observations were utilized as the input at the validation stage and the 1 km resolution
400 SMAPEX soil moisture data were used only for validation of the downscaled soil moisture.
401 Table 2 presents numerical information regarding the available data in the training and
402 validation phases.

403 The 12 columns were considered during the training of the machine learning algorithm,
404 which include the 11 input variables (available at 1 km or resampled to 1 km) and the one
405 output response variable (1 km ground soil moisture data). As an example, the focus area of
406 SMAPEX-3 provides a data set with 162 rows and 12 columns, where the 162 is computed as
407 $2 \times 9 \times 9$, with 2 referring to the number of ground sampling focus areas with an available dataset
408 for each day, 9 refers to the number of 1 km grid cells at each focus area (i.e., $3 \text{ km} \times 3 \text{ km}$),
409 and the last 9 refers to the number of experiment days during the campaign. The 11 input
410 variables were normalized from 0 to 1 before being utilized in both the training and validation

Table 2. Description of the data used for training and validation phases, including the number of 1 km grid cells, number of experiment days and the total available samples over selected campaigns.

| | Campaign | Number of 1 km grid cells | Number of experiment days | Total available samples |
|------------------|-----------------------|---------------------------|---------------------------|-------------------------|
| Training phase | SMAPE _x -3 | 18 | 9 | 162 |
| | SMAPVEX-12 | 25–50 | 16 | 585 |
| Validation phase | SMAPE _x -4 | 6035 | 6 | 33234 |
| | SMAPE _x -5 | 6319 | 8 | 50552 |

411 phases. This step was to remove any error due to the non-equal magnitudes of the input
 412 variables (Breiman 2001; O and Orth 2021; Srivastava et al. 2013). Subsequently, the SMAP
 413 soil moisture data was downscaled via the trained algorithm, utilizing the SMAPE_x-4 and
 414 SMAPE_x-5 data for the input variables. Finally, the SMAP downscaled soil moisture, was
 415 evaluated utilizing the ground soil moisture datasets and the high-resolution airborne
 416 radiometer derived soil moisture.

417 Fig. 3 presents a schematic of the proposed random forest model for downscaling the 36
 418 km SMAP soil moisture. The random forest algorithm requires the input variables on a 1 km
 419 grid. Therefore, the data collections which were not originally at 1 km resolution were
 420 resampled to this spatial resolution. The MATLAB built-in function TreeBagger from the
 421 MATLAB Regression Learner application was used to apply the random forest algorithm,
 422 working based on the Bagging (Bootstrap + Aggregating) approach (Breiman 1996, 2001).
 423 Using this method, the training dataset was sampled to M subgroups by the bootstrap approach,
 424 and the M individual regression decision trees fitted to train the random forest algorithm
 425 through using the input variable data. The predicted data was calculated through M replications.
 426 Finally, the average of the output values from the individual decision trees was considered as

427 the final result value. The ensemble decision was made by averaging the M results from
 428 individual regression trees:

$$p(SM_d|C) = \frac{1}{M} \sum_{t=1}^M p_t(SM_d|C), \quad (3)$$

429 where $p_t(SM_d|C)$ is the output of each individual decision tree determining the conditional
 430 distribution of the downscaled soil moisture (SM_d) considering the multidimensional feature
 431 input vector (C).

432 The k-fold cross-validation technique (Hastie et al. 2009) was also included in the model
 433 to avoid overfitting. A k-value equal to 5 was selected as it showed the best performance during
 434 the training, obtained through a trial and error approach. It is also important to choose the
 435 appropriate values for minimum leaf size and number of learners applied in the random forest
 436 model during the training phase to improve the downscaling accuracy. For this purpose,
 437 different values were tested through trial and error, with a minimum leaf size equal to nine and
 438 a number of learners equal to 25 yielding the best performance of the trained random forest
 439 model in improving the downscaling accuracy. After the training phase, the best calibrated
 440 random forest regression model was exported for implementation on the validation dataset,
 441 allowing the evaluation using unseen data. Accordingly, the SMAP radiometer soil moisture
 442 observations over the SMAP validation flight area (Fig. 1) were downscaled utilizing the
 443 calibrated random forest algorithm to 1 km resolution, and evaluated by the fine resolution
 444 ground soil moisture measurements at the focus areas averaged over 1 km grids, and also the
 445 soil moisture retrieved from the airborne brightness temperature at 1 km.

446 Validation of the downscaled soil moisture included quantification of statistical metrics and
 447 model errors, by comparing the estimated values with the airborne retrieved soil moisture
 448 observations and ground soil moisture measurements as the reference data. These metrics

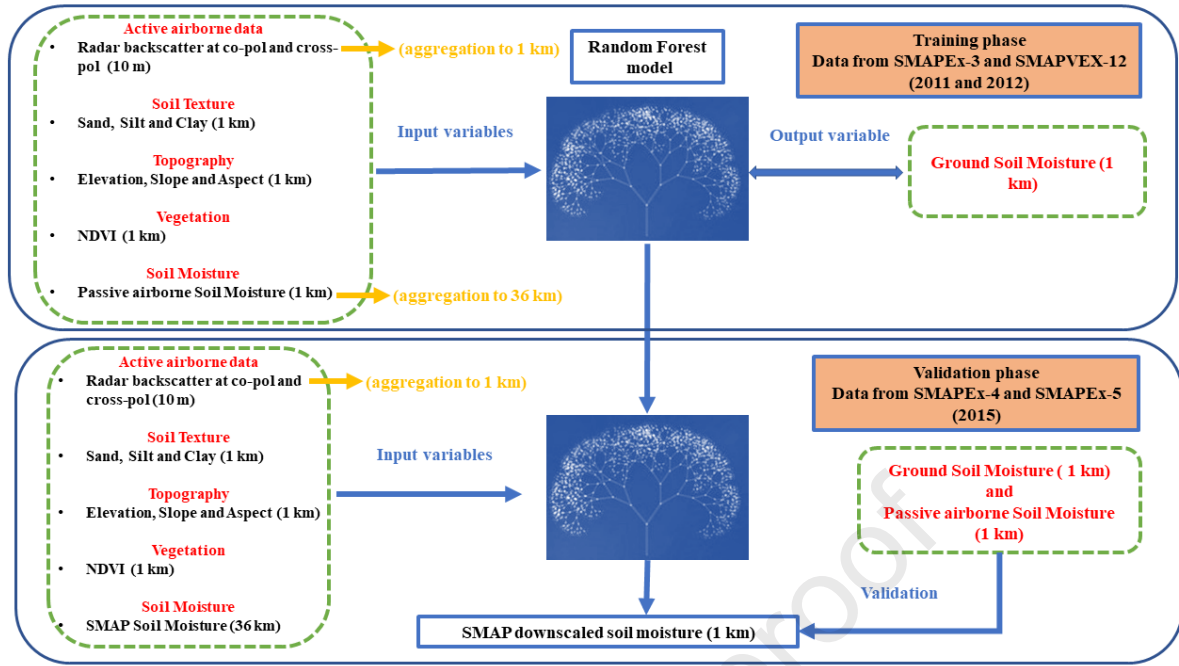


Fig.3. Flowchart of the proposed random forest downscaling model.

449 include the unbiased root mean square error ($ubRMSE$), Pearson correlation coefficient (R),
 450 and mean difference or bias. The $ubRMSE$ was considered as the representative accuracy of the
 451 soil moisture in this research.

452 The importance of each individual variable was assessed to analyze the relative
 453 contribution of input features on the random forest downscaling accuracy. For this purpose, a
 454 leave-one-out approach was performed by removing the one input variable (i.e., radar
 455 backscatter, NDVI, DEM, terrain slope and aspect, soil texture) and implementing the random
 456 forest downscaling algorithm using the rest of the variables in order to investigate the impact
 457 of the removed variable.

458 5. Results and discussion

459 5.1. Evaluation of the soil moisture data sets

460 Original SMAP_L3, PLMR and PALS soil moisture observations (resampled to 1 km
 461 spatial resolution) were first evaluated against the ground soil moisture measured during the

462 experiment periods. Fig. 4 demonstrates the evaluation of the different soil moisture
463 observations against ground soil moisture measurements at the pixel level, including the
464 statistical analysis values. Accordingly, the correlation coefficients between the PALS and
465 PLMR retrieved soil moisture with the ground measurement were found to be higher than the
466 SMAP_L3 soil moisture by $0.03 \text{ m}^3 \cdot \text{m}^{-3}$ and $0.07 \text{ m}^3 \cdot \text{m}^{-3}$ for PLMR and PALS, respectively.
467 In contrast, the original SMAP_L3 soil moisture showed better *ubRMSE* against ground
468 measurements than the airborne soil moisture retrieval from PLMR and PALS, achieving the
469 lowest value equal to $0.062 \text{ m}^3 \cdot \text{m}^{-3}$. The highest *ubRMSE* was obtained between PLMR soil
470 moisture retrieval and ground observations as $0.09 \text{ m}^3 \cdot \text{m}^{-3}$, which was partially due to standing
471 water found in grasslands (due to heavy rainfall) at the beginning of the SMAPEX-5 campaign
472 and crop lands (due to flood irrigation) at the end of the SMAPEX-5 campaign. Importantly,
473 the PLMR instrument captured the soil moisture variation of these pixels. The calculation of
474 bias statistics showed an overestimation for SMAP_L3 soil moisture of $0.013 \text{ m}^3 \cdot \text{m}^{-3}$, and an
475 underestimation for PLMR and PALS soil moisture of $-0.008 \text{ m}^3 \cdot \text{m}^{-3}$ and $-0.029 \text{ m}^3 \cdot \text{m}^{-3}$
476 respectively when compared against ground measurements.

477 For comparison, the SMAP_L3 soil moisture has been resampled to 1 km resolution by
478 applying the same soil moisture value for each 1 km pixel within each 36 km EASE grid cell.
479 The resampled SMAP soil moisture has then been compared against the PLMR soil moisture
480 obtained during the SMAPEX-4 and -5 experiments. This is considered as the “do-nothing”
481 baseline performance that the downscaling algorithm must beat in order to add value. Fig. 5
482 shows that the comparison had a correlation coefficient of 0.66, bias of $0.016 \text{ m}^3 \cdot \text{m}^{-3}$
483 (SMAP_L3 higher), and *ubRMSE* of $0.121 \text{ m}^3 \cdot \text{m}^{-3}$. Thus, in order to ensure that the differences
484 between the SMAP downscaled soil moisture and the airborne retrieved soil moisture at high
485 spatial resolution were affected only by the machine learning downscaling algorithm, and not

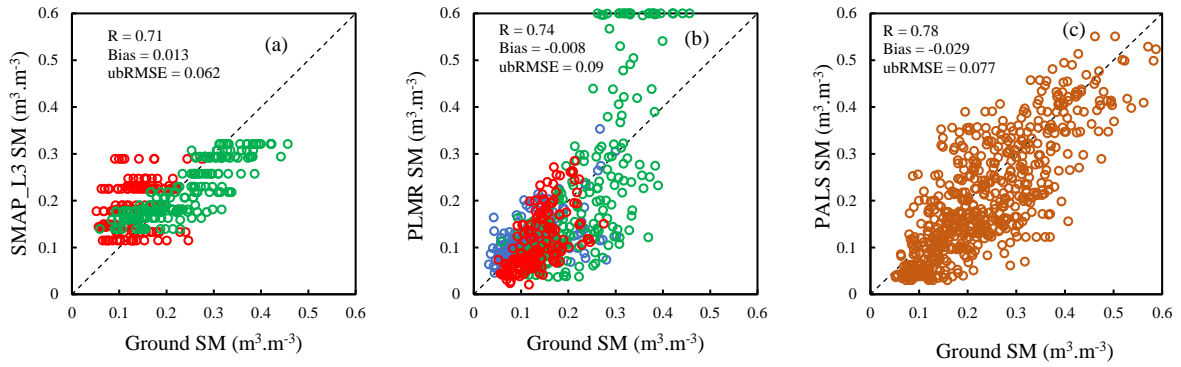


Fig. 4. Evaluation of different soil moisture observations against ground soil moisture measurements including a) 36 km SMAP_L3 SM during 30 April – 23 May, 2015 (SMAPEX-4, red points) and 6–28 September, 2015 (SMAPEX-5, green points) at the SMAPEX-4 and -5 sites, respectively; b) 1 km PLMR SM during 5–23 September, 2011 (SMAPEX-3, blue points), 30 April – 23 May, 2015 (SMAPEX-4, red points) and 6–28 September, 2015 (SMAPEX-5, green points) at the SMAPEX-3, -4 and -5 sites, respectively; and c) 1 km PALS SM during 7 June – 19 July, 2012 at the SMAPVEX-12 site (SMAPVEX-12, brown points).

486 because of the sensor to sensor bias, this bias value between the SMAP and PLMR soil moisture
 487 was removed before utilizing the data in the downscaling process.

488 5.2. Results from random forest model development

489 The calibration and validation of the proposed random forest algorithm was conducted
 490 using the input and output variables over selected areas. As mentioned earlier, the normalized
 491 training dataset from the SMAPEX-3 and SMAPVEX-12 experiments was partitioned into a 5-
 492 fold cross-validation. In the training phase, the 1 km ground soil moisture dataset was used in
 493 the algorithm for matching with the output response variable (see Fig. 3). The statistical results
 494 of the Ensemble TreeBagger algorithm applied at the training phase showed a good
 495 performance with R , root mean square error ($RMSE$) and mean absolute error (MAE) of 0.88,
 496 $0.05 \text{ m}^3.\text{m}^{-3}$ and $0.04 \text{ m}^3.\text{m}^{-3}$, respectively, demonstrating the capability of the calibrated

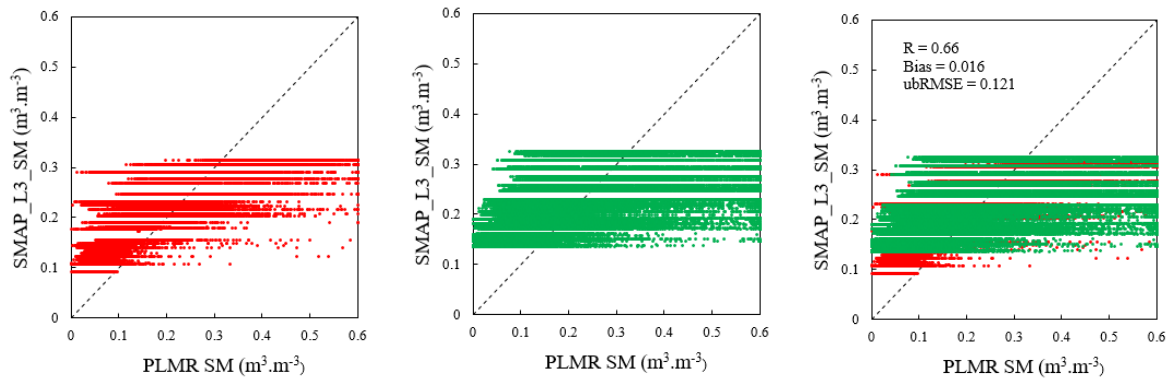


Fig. 5. Comparison of SMAP_L3 SM resampled to 1 km against 1km PLMR airborne soil moisture retrieval during 30 April – 23 May, 2015 (SMAPEX-4, red points) and 6–28 September, 2015 (SMAPEX-5, green points) over SMAPEX-4 and SMAPEX-5 flight areas, respectively.

497 random forest model for generalization to an unseen dataset. These results showed a better
 498 correlation coefficient and *RMSE* than Senanayake et al. (2021), which used the Gaussian
 499 process regression model over the Yanco area for downscaling of soil moisture. The statistical
 500 results of this research have been obtained by trying different numbers of decision trees and
 501 tree leaf size to achieve a suitable calibrated random forest model for the downscaling.

502 5.3. Assessment of the downscaling algorithm performance

503 5.3.1. Comparison of downscaled soil moisture with PLMR airborne retrieved data

504 Fig. 6 provides the scatterplots and statistical results of the SMAP downscaled soil moisture
 505 against PLMR soil moisture observations, which exhibit good agreements. The calculated *R*,
 506 bias, and *ubRMSE* were 0.97, 0.016 $\text{m}^3.\text{m}^{-3}$ and 0.048 $\text{m}^3.\text{m}^{-3}$. The results show the
 507 improvement of *R* from 0.66 between the SMAP_L3 and PLMR soil moisture to 0.97 between
 508 the downscaled SMAP and PLMR soil moisture. Importantly, when utilizing the random forest
 509 algorithm trained only by the SMAPVEX-12 data there was no apparent degradation in the
 510 downscaled results (results not shown) when applied to the SMAPEX data, even though applied

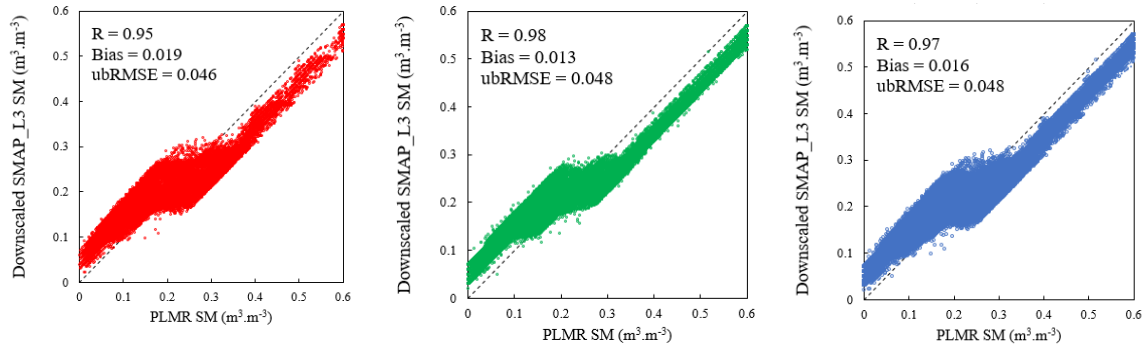


Fig. 6. Validation of downscaled SMAP soil moisture versus PLMR airborne soil moisture retrieval (1 km) during 30 April – 23 May, 2015 (SMAPEX-4, red points) and 6–28 September, 2015 (SMAPEX-5, green points) and all available data (blue points) over PLMR flight areas. All available data (blue points) include both SMAPEX-4 (red points) and SMAPEX-5 (green points) data.

511 to an entirely independent site, suggesting that there is some degree of transferability of the
 512 machine learning approach to locations different to those used for training. Additionally, the
 513 random forest algorithm was trained utilizing data over the entire flight areas of the SMAPEX-
 514 3 (36 km × 38 km) and SMAPVEX-12 (12.8 km × 70 km) study areas (Fig. 2) on experiment
 515 days. In this case, the calculated R , bias, and $ubRMSE$ between the downscaled SMAP soil
 516 moisture using the random forest model and PLMR soil moisture of SMAPEX-4 and SMAPEX-
 517 5 were 0.97, 0.015 $\text{m}^3.\text{m}^{-3}$ and 0.051 $\text{m}^3.\text{m}^{-3}$, being only slightly different from the results
 518 reported in Fig. 6. However, the scatter plots indicate an overestimation at lower soil moisture
 519 values, and an underestimation between downscaled SMAP soil moisture and PLMR values at
 520 higher soil moisture values. Importantly, $ubRMSE$, the main statistical metric of the
 521 downscaling algorithm accuracy, improved from 0.121 $\text{m}^3.\text{m}^{-3}$ to 0.048 $\text{m}^3.\text{m}^{-3}$, showing good
 522 downscaling performance by the proposed random forest model.

523 Overall, the statistical results achieved through the comparison of the downscaled SMAP
 524 pixel with the PLMR soil moisture showed the success of the developed random forest
 525 algorithm in downscaling the SMAP soil moisture. The results of the random forest method

526 utilized in this study are encouraging, especially when evaluated with the results of the original
527 SMAP soil moisture reported in Fig. 5, with an improved accuracy of downscaled SMAP soil
528 moisture against PLMR measurements, and the results of earlier studies shown in Sabaghy et
529 al. (2020) for the same site. Consequently, the quality of PLMR observations and their full
530 spatial coverage over the selected area have provided a good opportunity to investigate machine
531 learning based downscaling.

532 In order to assess the soil moisture spatial distribution, the spatial pattern of SMAP
533 downscaled soil moisture were investigated against the course resolution SMAP observations
534 and the airborne retrieved soil moisture. Figs. 7 and 8 present the spatial variability in the
535 downscaled, original SMAP soil moisture, and PLMR retrieved soil moisture over the SMAP
536 validation flight area of SMAPEX-4 (71 km × 85 km) and SMAPEX-5 (71 km × 89 km) during
537 each of the experiment days (D is representative of the day). The downscaled maps closely
538 correspond to the airborne soil moisture retrieval patterns. The rainfall events on 9th and 18th
539 May (D3 and D5) during SMAPEX-4 were clearly captured by the spatial pattern, as the soil
540 moisture in these days showed higher values than others (Fig. 7). The dry down pattern during
541 SMAPEX-5 from D1 to D8 corresponds to the rainfall events that preceded the campaign (Fig.
542 8). Overall, the downscaled soil moisture closely matched the pattern of the PLMR
543 observations during both the SMAPEX-4 and SMAPEX-5 experiments, conducted under
544 diverse climate and vegetation conditions.

545 To further analyse the capability of the downscaling model at capturing the soil moisture
546 change, the pattern of the temporal variation of the SMAP downscaled and airborne soil
547 moisture was investigated. There were several heavy rainfall events before both the SMAPEX-
548 4 and SMAPEX-5 campaigns, providing heterogeneous soil moisture conditions with dry
549 downs. Furthermore, the two additional rainfall events on the 9th and 18th of May during the
550 SMAPEX-4 experiments are visible in Fig. 7 as increased soil moisture values. In contrast,

551 there was no significant additional rainfall during SMAPEX-5, resulting in a prolonged dry
552 down. Figs. 7 and 8 show that both the SMAP course resolution and the downscaled soil
553 moisture values correspond to the temporal variability of the PLMR soil moisture in response
554 to rainfall events. For instance, the higher amounts of soil moisture at the beginning of
555 SMAPEX-5 are attributed to rainfall followed by a dry down with a distinct soil moisture
556 pattern that is clearly detected. However, the consistency of the original and downscaled SMAP
557 soil moisture with the PLMR soil moisture was affected based on the land cover and
558 atmospheric situations. In the following, the differences are discussed according to the soil
559 moisture dynamic ranges. For this purpose, the minimum and maximum amounts of soil
560 moisture have been mentioned to clarify the ranges of the soil moisture.

561 Over the SMAPEX-4 site, the original and downscaled SMAP soil moisture varied from
562 $0.09 \text{ m}^3.\text{m}^{-3}$ to $0.31 \text{ m}^3.\text{m}^{-3}$ and from $0.022 \text{ m}^3.\text{m}^{-3}$ to $0.57 \text{ m}^3.\text{m}^{-3}$, respectively. Over the
563 SMAPEX-5 site, the SMAP course resolution and downscaled soil moisture varied from 0.13
564 $\text{m}^3.\text{m}^{-3}$ to $0.33 \text{ m}^3.\text{m}^{-3}$ and from $0.02 \text{ m}^3.\text{m}^{-3}$ to $0.57 \text{ m}^3.\text{m}^{-3}$, respectively. Overall, the range of
565 downscaled SMAP soil moisture was more than the range of the original SMAP soil moisture
566 over SMAPEX-4 and SMAPEX-5. In addition, the PLMR soil moisture ranged from $0 \text{ m}^3.\text{m}^{-3}$
567 to $0.6 \text{ m}^3.\text{m}^{-3}$ during SMAPEX-4 and SMAPEX-5. According to Figs. 7 and 8, it can be seen
568 that the soil was generally wetter and with larger range during SMAPEX-5 than SMAPEX-4.
569 Moreover, the vegetation water content was high with actively growing vegetation, and
570 agricultural activities such as irrigation affecting the soil moisture ranges and the standing
571 water, leading to increased PLMR retrieval uncertainties for some pixels. In order to minimize
572 these errors, the bias value between the original SMAP soil moisture and the PLMR retrieved
573 soil moisture was removed.

574 To investigate the spatial distribution of errors during the downscaling process, the actual
575 difference plots between the downscaled SMAP soil moisture and PLMR observations have

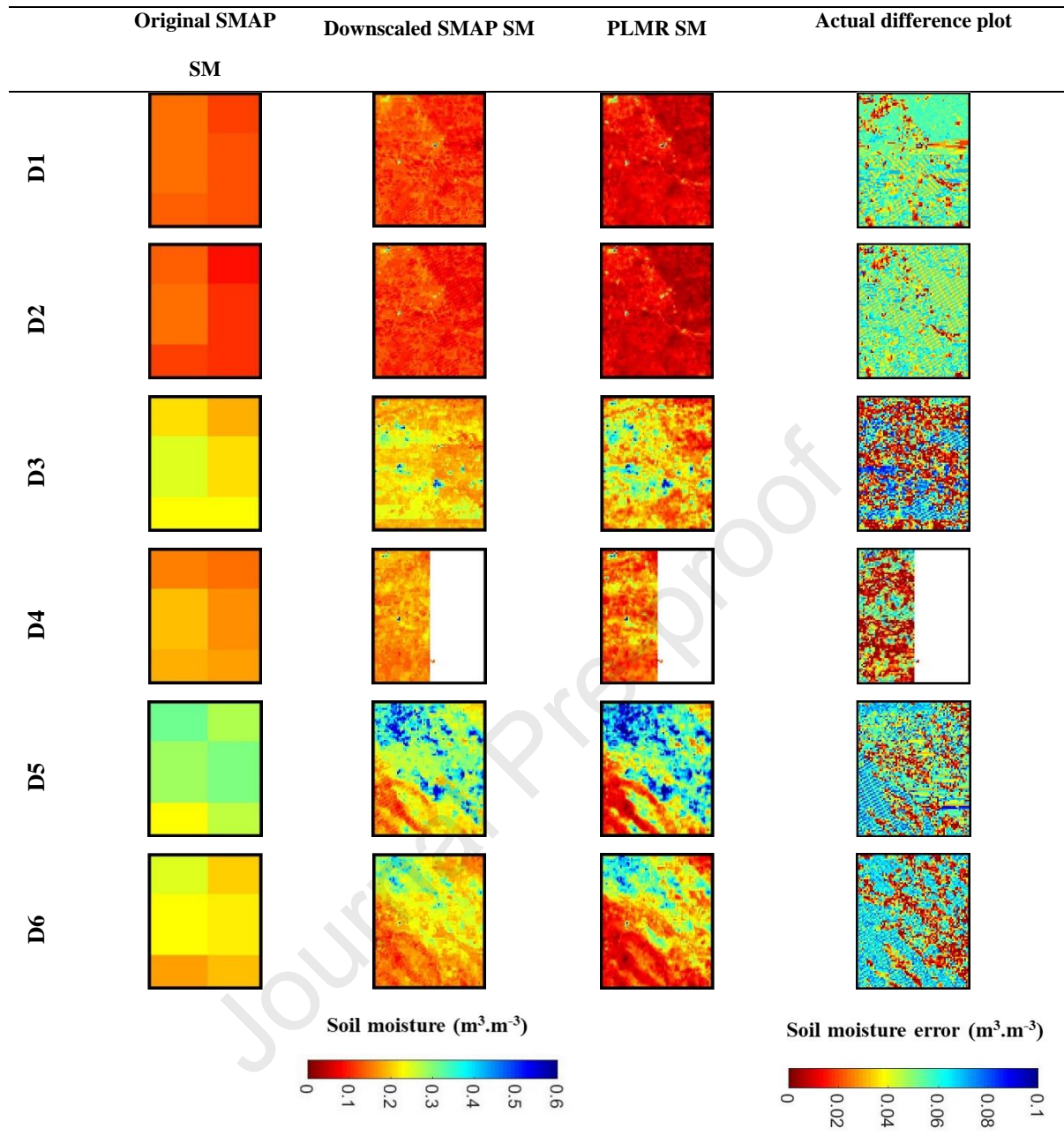


Fig. 7. Spatial distribution of original SMAP_L3 soil moisture (36 km), downscaled SMAP soil moisture (1 km), and airborne PLMR retrieved soil moisture (1 km) at 5 cm depth during the period 30 April – 23 May, 2015 at SMAPEX-4 over PLMR flight area (71 km \times 85 km).

576 also been presented in Figs. 7 and 8. Overall, the difference values gave good agreement
 577 between PLMR and downscaled soil moisture, but showed that the errors between PLMR and
 578 downscaled products at the dry and wet soil moisture conditions had more bias than under more
 579 normal soil moisture situations.

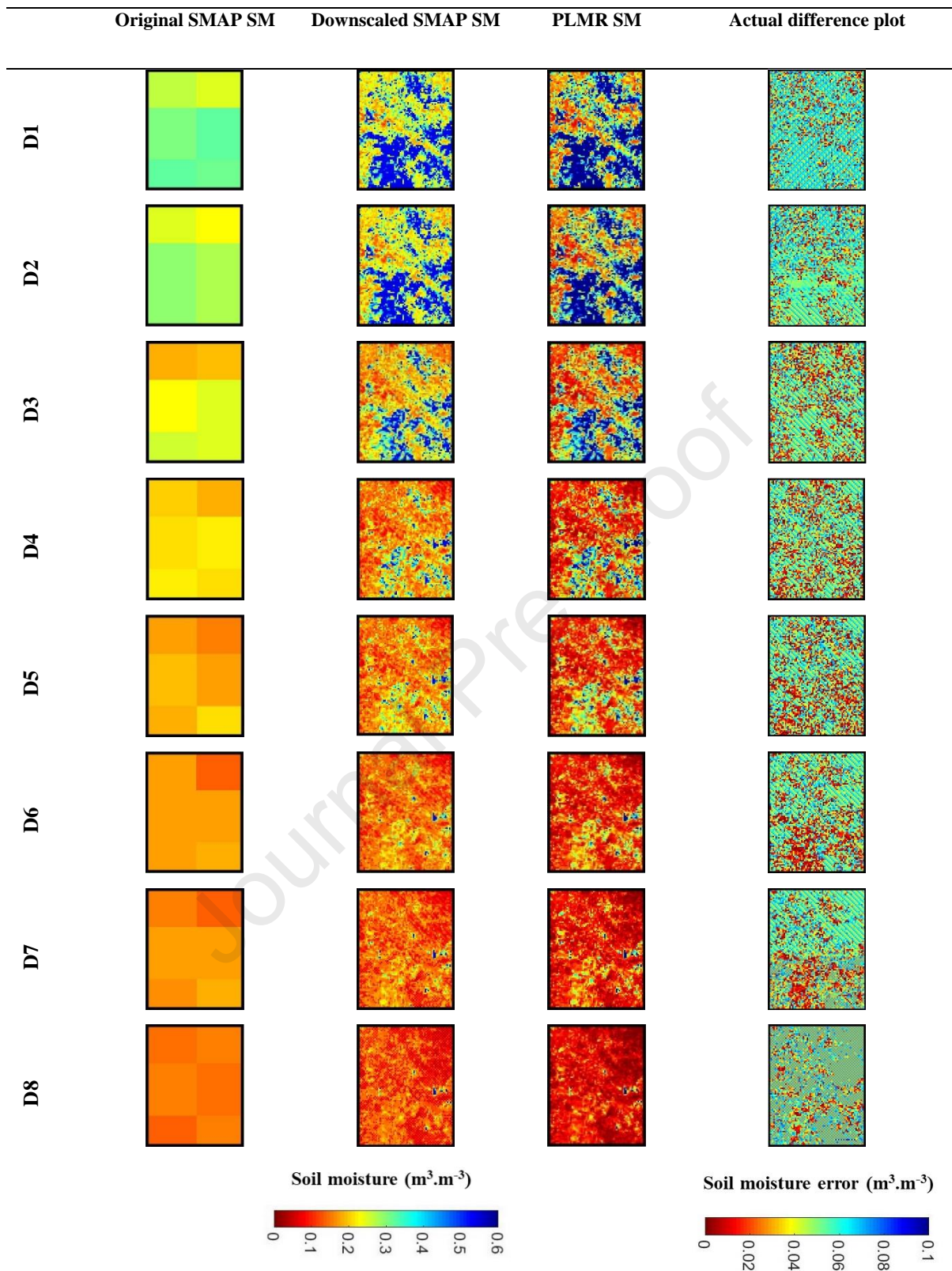


Fig. 8. Same as Fig. 7 except for SMAPEX-5 over PLMR flight area ($71 \text{ km} \times 89 \text{ km}$) during the period 6–28 September, 2015.

580 5.3.2. Comparison of downscaled soil moisture with ground measurements

581 The calculated R , bias, and $ubRMSE$ of the downscaled SMAP soil moisture against the
 582 ground data were 0.73, $-0.047 \text{ m}^3 \cdot \text{m}^{-3}$ and $0.057 \text{ m}^3 \cdot \text{m}^{-3}$ for clay loam, 0.83, $-0.038 \text{ m}^3 \cdot \text{m}^{-3}$ and
 583 $0.072 \text{ m}^3 \cdot \text{m}^{-3}$ for loam, and 0.8, $-0.031 \text{ m}^3 \cdot \text{m}^{-3}$ and $0.06 \text{ m}^3 \cdot \text{m}^{-3}$ for silty clay loam (Fig. 9). The
 584 statistical results demonstrated that the downscaled soil moisture had a good correlation with
 585 the ground soil moisture observations over these soil texture conditions, especially for loam
 586 and silty clay loam textures, and an underestimation of downscaled soil moisture over all of
 587 the selected soil texture conditions. The $ubRMSE$ showed better performance for the clay loam
 588 and silty clay loam soil textures than the loam soil texture condition.

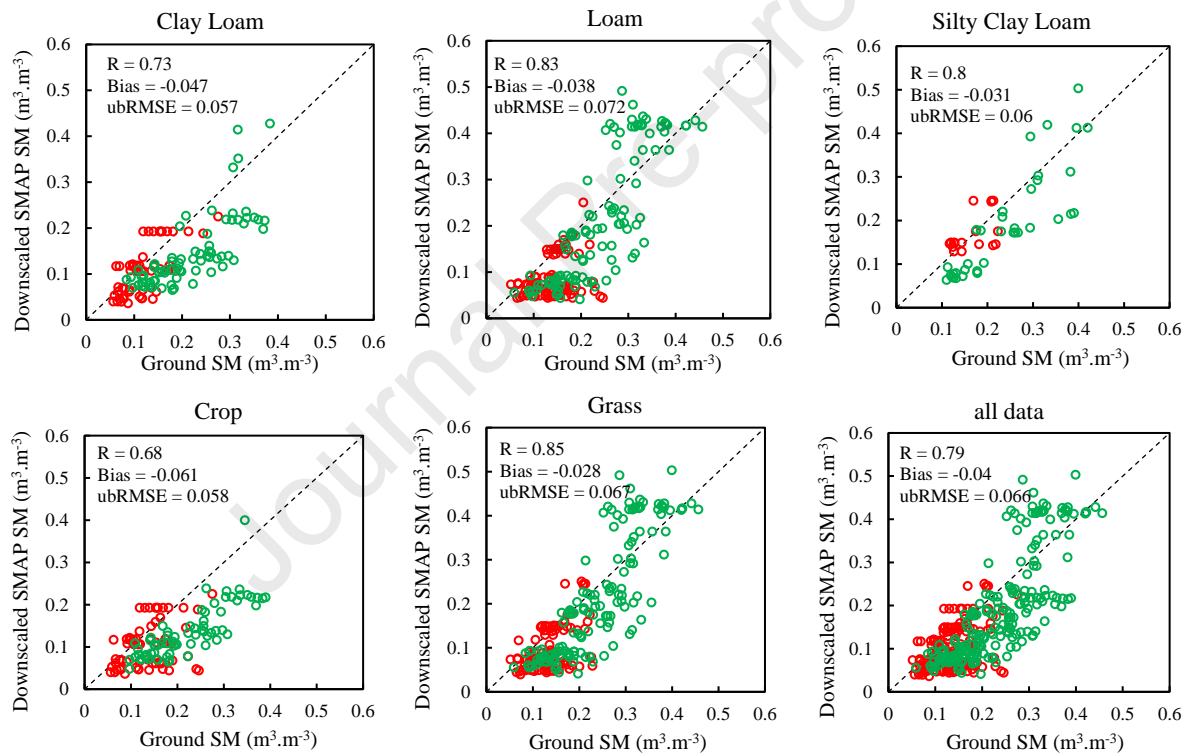


Fig. 9. Validation of downscaled SMAP soil moisture versus ground soil moisture measurements (1 km) over the SMAPEX focus area during 30 April – 23 May, 2015 (SMAPEX-4, red points) and 6–28 September, 2015 (SMAPEX-5, green points). The first row presents the results for different soil texture conditions, and the second row shows the results for different land cover types, along with the results from all available data.

589 The performance of the downscaled SMAP soil moisture was also assessed considering the
590 two types of land covers. The R , bias, and $ubRMSE$ were 0.68, $-0.061 \text{ m}^3 \cdot \text{m}^{-3}$ and $0.058 \text{ m}^3 \cdot \text{m}^{-3}$
591 3 for the cropland, and 0.85, $-0.028 \text{ m}^3 \cdot \text{m}^{-3}$ and $0.067 \text{ m}^3 \cdot \text{m}^{-3}$ for the grassland (Fig. 9). The bias
592 was negative (downscaled SMAP soil moisture lower) for both cropland and grassland, and
593 although the R was worse for the cropland than for the grassland, the $ubRMSE$ was better for
594 the cropland than for the grassland.

595 The R , bias, and $ubRMSE$ were 0.79, $-0.04 \text{ m}^3 \cdot \text{m}^{-3}$ and $0.066 \text{ m}^3 \cdot \text{m}^{-3}$ for all data over
596 selected focus areas (Fig. 9). Although the R was better compared with those for SMAP_L3
597 (Fig. 4), the $ubRMSE$ was not better in this case. Overall, the results of this study are consistent
598 with those from Abbaszadeh et al. (2019), which utilized the random forest approach for SMAP
599 soil moisture downscaling over the Continental United States at different soil texture
600 conditions.

601 For a more detailed investigation, the performance of the downscaled SMAP soil moisture
602 was assessed with the SMAPEX-4 and SMAPEX-5 data separately. Because these campaigns
603 were conducted in different seasons, they provide insight into the effects of different
604 atmospheric conditions, soil moisture variations, and variability in vegetation. The SMAPEX-
605 4 data was collected in the austral autumn with the land surface type of bare soil in croplands
606 and grasslands covered by short grass. In comparison, the SMAPEX-5 took place during the
607 austral spring when the crops were in the growth stage with high vegetation water content, and
608 grassland vegetation was at mature stages, as described earlier. Table 3 reports the statistical
609 analysis, including R , bias, and $ubRMSE$ between the downscaled SMAP soil moisture and
610 ground measurements considering the soil texture and land cover scenarios for SMAPEX-4 and
611 SMAPEX-5 experiments. The R showed good values for all scenarios of the SMAPEX-5
612 experiment. Moreover, R showed acceptable values for the SMAPEX-4 experiment with the
613 exception of loam soil texture and croplands. While the $ubRMSE$ values meet the SMAP soil

Table 3. The statistical metrics of soil moisture comparison between ground soil moisture and SMAP downscaled estimates according to land cover and soil texture during SMAPEX-4 and SMAPEX-5, separately.

| Campaign name | | SMAPEX-4 | | | SMAPEX-5 | | |
|---------------|------------------------|----------|----------------------------|----------------------------|----------|----------------------------|----------------------------|
| | | <i>R</i> | Bias | <i>ubRMSE</i> | <i>R</i> | Bias | <i>ubRMSE</i> |
| | | - | $\text{m}^3.\text{m}^{-3}$ | $\text{m}^3.\text{m}^{-3}$ | - | $\text{m}^3.\text{m}^{-3}$ | $\text{m}^3.\text{m}^{-3}$ |
| Soil texture | Clay Loam | 0.76 | -0.013 | 0.04 | 0.68 | -0.073 | 0.055 |
| | Loam | 0.27 | -0.055 | 0.051 | 0.82 | -0.026 | 0.084 |
| | Silty Clay Loam | 0.56 | 0.005 | 0.038 | 0.86 | -0.048 | 0.062 |
| Land Cover | Crop | 0.36 | -0.034 | 0.059 | 0.82 | -0.086 | 0.046 |
| | Grass | 0.53 | -0.034 | 0.046 | 0.84 | -0.025 | 0.078 |

614 moisture accuracy requirement for nearly all selected soil texture and land cover situations over
 615 SMAPEX-4, the *ubRMSE* over SMAPEX-5 showed worse values than SMAPEX-4 results,
 616 except for the cropland situation.

617 Overall, considering the ground soil moisture measurements as an independent reference,
 618 the proposed random forest model improved the accuracy of downscaled SMAP soil moisture
 619 over the focus areas of SMAPEX-4, when comparing with the uniform values from the original
 620 SMAP_L3 product. However, the statistics of the downscaled SMAP soil moisture did not
 621 show equal improvement for the focus areas of SMAPEX-5. It seems that at these focus areas,
 622 the downscaling performance was affected by the high vegetation water content and flood
 623 irrigation during the SMAPEX-5 experiments.

624 Fig. 10 and Fig. 11 present the spatial variability of the downscaled and original SMAP_L3
 625 soil moisture, and ground soil moisture measurements over the $3 \text{ km} \times 3 \text{ km}$ SMAPEX focus
 626 areas of SMAPEX-4 and SMAPEX-5 during each of the experimental days. The downscaled
 627 soil moisture maps correspond to the patterns of the ground soil moisture observations by

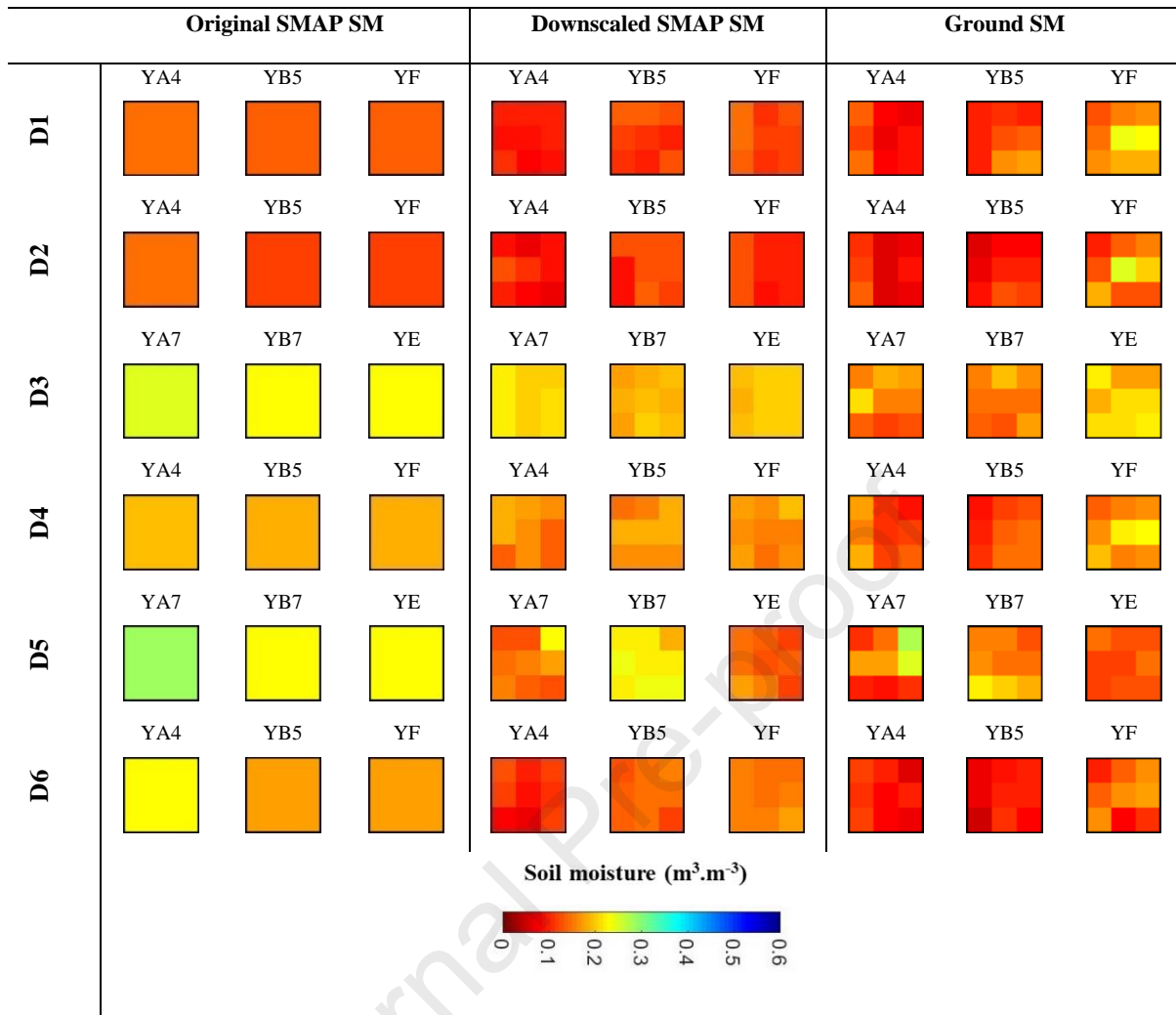


Fig. 10. Spatial distribution of original SMAP_L3 soil moisture (36 km), downscaled SMAP soil moisture (1 km) and ground soil moisture (1 km) measurements at 5 cm depth during the period 30 April – 23 May, 2015 at SMAPEX-4 focus areas (3 km \times 3 km).

628 generally capturing the rainfall events during SMAPEX-4 (Fig. 10) and the dry down pattern
 629 of SMAPEX5 due to the rainfall events prior to the campaign (Fig. 11).

630 The geographic parameters such as topography, vegetation coverage, and soil texture
 631 contribute to the heterogeneity. While the topography of the SMAPEX focus areas does not
 632 change substantially, there are three distinct soil texture types. Considering the spatial
 633 distribution based on the soil textures for SMAPEX-4 (Fig. 10), the downscaled soil moisture
 634 matched the spatial pattern of the ground soil moisture qualitatively for different soil texture
 635 conditions. Considering the spatial distribution based on the land cover of SMAPEX-4, it seems

636 that the spatial distribution of soil moisture within the focus area under both grassland and
 637 cropland showed good consistency when compared to the ground soil moisture measurements.
 638 It is notable that conditions included bare soil in the cropland and sparsely vegetated dry
 639 grassland during the SMAPEX-4 experiment. These conditions will have affected the soil
 640 drying states as well as rapid infiltration after any rainfall or irrigation.

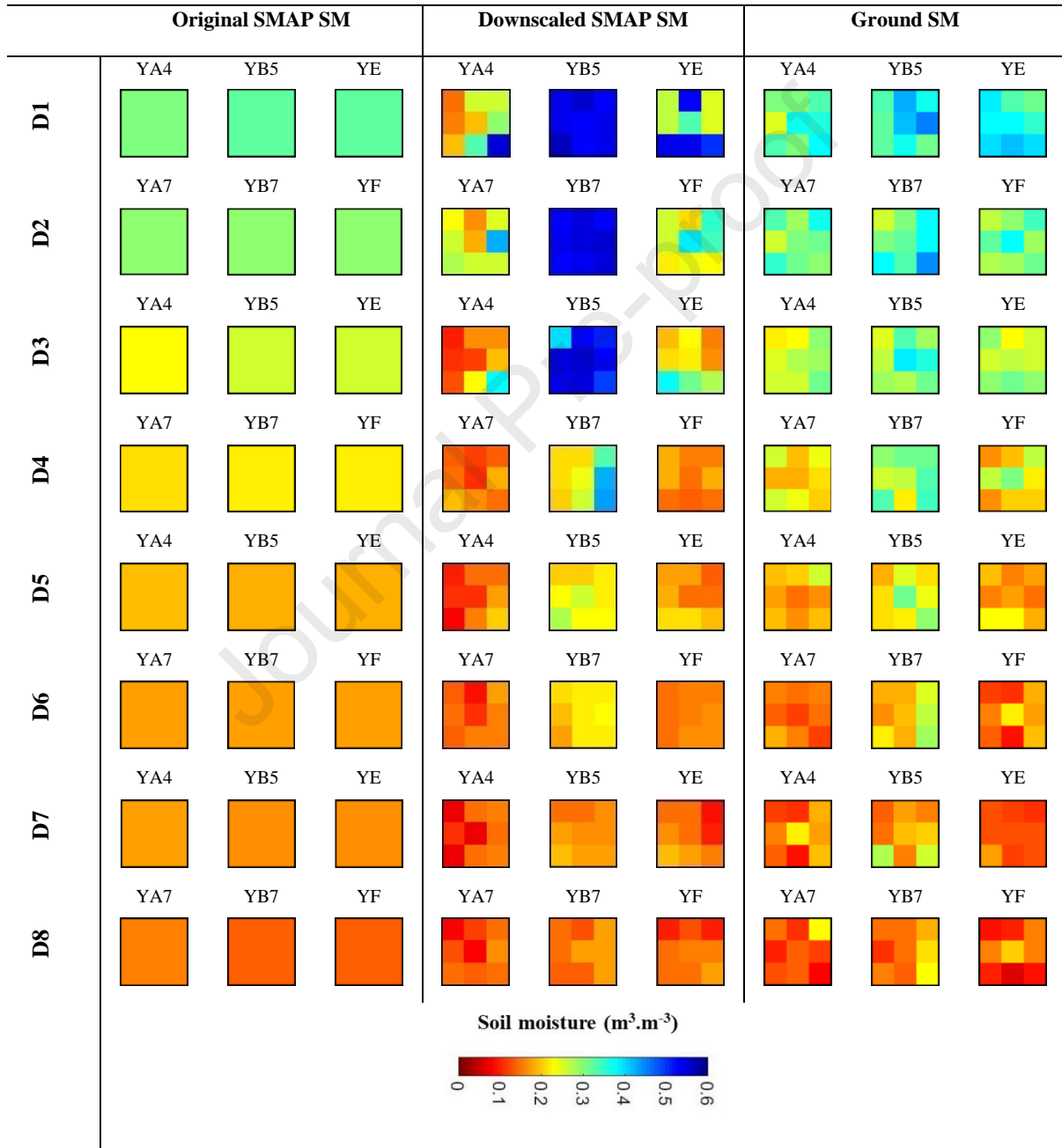


Fig. 11. Same as Fig. 10 except for SMAPEX-5 focus areas ($3 \text{ km} \times 3 \text{ km}$) during the period 6–28 September, 2015.

641 Based on the spatial distribution maps, greater heterogeneity in the soil moisture spatial
642 distribution was visible for vegetated and irrigated areas during SMAPEX-5. However, the
643 greater vegetation led to an increased attenuation of the microwave signal, contributing to an
644 underestimation of soil moisture. Considering the spatial distribution in the different soil
645 texture variations, for SMAPEX-5 (Fig. 11) the downscaled soil moisture matched qualitatively
646 the spatial pattern of the ground soil moisture for the clay loam texture type (YA4, YA7).
647 Moreover, considering the spatial distribution based on the land cover of SMAPEX-5, the soil
648 moisture spatial distribution of the focus area showed qualitatively better consistency under
649 croplands (YA4 and YA7) than grasslands. The random forest method showed higher
650 uncertainty under grassland (YB5 and YB7) in downscaling the SMAP soil moisture during
651 the early days of the campaign, which were influenced by standing water. Table 3 reports the
652 same results, with the *ubRMSE* values over SMAPEX-5 achieving $0.046 \text{ m}^3 \cdot \text{m}^{-3}$ and 0.078
653 $\text{m}^3 \cdot \text{m}^{-3}$ for cropland and grassland, respectively.

654 **5.4. Results of utilizing 36 km SMAP data at 1 km in the training phase**

655 Most of the machine learning based passive soil moisture downscaling approaches to date
656 have focused on utilizing the coarse resolution grid cell soil moisture uniformly across all fine
657 resolution grid cells as an input in the training phase. In order to understand the effect of such
658 assumptions, the results from utilizing the 1 km soil moisture values at the focus areas were
659 compared with results from utilizing 36 km grid cell average soil moisture at the same focus
660 areas as the input in the training phase of the random forest algorithm. Fig. 12 shows the scatter
661 plots and the statistical analysis of the downscaled SMAP soil moisture against airborne PLMR
662 soil moisture and the ground soil moisture measurements for the two different approaches over
663 the ground sampling focus area. When using the average soil moisture of the 36 km grid cell
664 as the input in the training phase, the statistical metrics *R*, bias, and *ubRMSE* of the SMAP
665 downscaled soil moisture against PLMR soil moisture were 0.53, $0.055 \text{ m}^3 \cdot \text{m}^{-3}$, and 0.083

666 $\text{m}^3.\text{m}^{-3}$, and against ground soil moisture were 0.54, 0.014 $\text{m}^3.\text{m}^{-3}$ and 0.074 $\text{m}^3.\text{m}^{-3}$. The
667 accuracy of the downscaled SMAP soil moisture derived from the random forest algorithm
668 based on the proposed approach of this paper clearly showed better performance in *ubRMSE*
669 (by 0.04 $\text{m}^3.\text{m}^{-3}$) than the algorithm based on utilizing the averaged soil moisture. Additionally,
670 the range of downscaled soil moisture based on utilizing the average soil moisture changed
671 from 0.02 $\text{m}^3.\text{m}^{-3}$ to 0.15 $\text{m}^3.\text{m}^{-3}$, which was substantially lower than the range of downscaled
672 soil moisture based on the proposed approach. Overall, utilizing 1 km grid soil moisture
673 observations as the input in the training phase showed a better skill level in matching with
674 observed soil moisture patterns, meaning that it can construct a well-trained downscaling
675 algorithm.

676 **5.5. Importance of input variables to the downscaled soil moisture**

677 The importance of different variables must be analysed in order to realize their
678 effectiveness on the performance of the random forest algorithm for soil moisture downscaling.
679 In random forest models, the increased percentage of *MSE* in comparison with that achieved
680 from utilizing all variables in the model describes the importance of different variables. When
681 an important variable is not used in the algorithm, the *MSE* will increase, with the larger the
682 increase in *MSE* signifying the greater the importance of that variable (Breiman 2001).
683 Therefore, the significance of each input variable was analysed using the ablation test, in which
684 each input variable was independently omitted from the downscaling process and the random
685 forest algorithm applied using the remaining variables. Ten different input schemes including
686 removal of the radar backscatter (σ_{vv} , σ_{hh} , σ_{xpol}), NDVI, DEM, slope, aspect and soil texture (%
687 clay, silt and sand) were tried independently. Removal of soil moisture from the input variables
688 increased the percentage of *MSE* value equal to 23.8 %, showing the highest importance in this
689 machine learning downscaling approach. Therefore, as downscaling of the SMAP soil moisture
690 was the main purpose of this research, the soil moisture parameter was included in the input

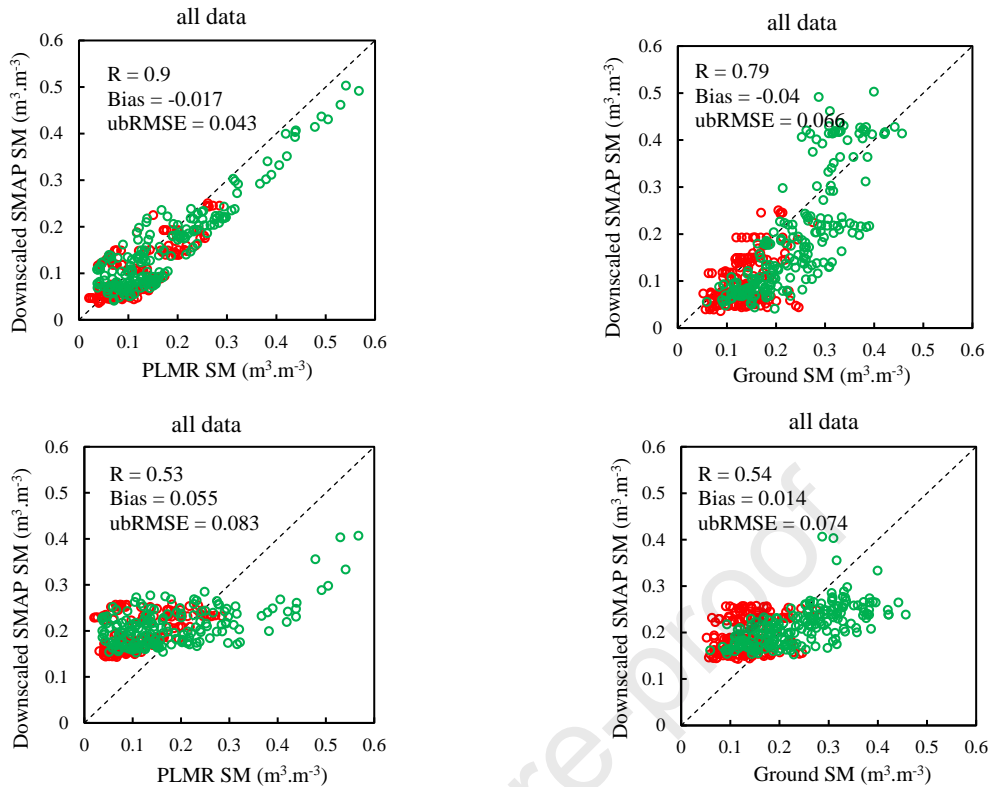


Fig. 12. Validation of downscaled SMAP soil moisture against airborne PLMR retrieved soil moisture (1 km) and ground soil moisture measurements (1 km) over the SMAPEX focus areas during 30 April – 23 May, 2015 (SMAPEX-4, red points) and 6–28 September, 2015 (SMAPEX-5, green points). The first row presents the results for utilizing 1 km soil moisture at focus areas as the input in the training phase, and the second row shows the results for utilizing the average soil moisture of the 36 km grid cell as the input in the training phase.

691 schemes. The *MSE* values of the downscaled SMAP soil moisture estimates relative to PLMR
 692 soil moisture were calculated separately for each input variable, with percentage of increase in
 693 *MSE* values shown in Fig. 13.

694 Horizontal backscatter (σ_{hh}) and slope are recognized as the most important variables (3.66
 695 % and 3.63 %, respectively), showing more influence than other variables on the random forest
 696 accuracy. Soil texture ranked third, indicating 2.85 % and 2.76 % importance for sand and clay,
 697 respectively. The soil texture can influence water permeability, infiltration rate and water
 698 storage capacity. In this assessment, silt fraction showed least importance compared to other

699 input variables in the proposed downscaling model. NDVI also showed high importance (2.51
700 %) due to the ability of presenting the vegetation status; NDVI is one of the crucial auxiliary
701 parameters used in soil moisture retrieval, and in several soil moisture downscaling algorithms
702 (Colliander et al. 2017a; Colliander et al. 2017b). Among the airborne co-polarized and cross-
703 polarized backscatter products utilized in the random forest model, the importance of horizontal
704 co-polarized backscatter (σ_{hh}) was highest (3.66 %). However, the vertical co-polarized
705 backscatter (σ_{vv}) and cross-polarized backscatter (σ_{hv}) also showed a high influence. While the
706 DEM had a slightly lower influence (1.73 %) compared to the high influence input variables
707 on the results, it is one of the important input variables in the proposed random forest algorithm
708 in this study. However, previous research has shown the high importance of a vegetation index
709 such as NDVI in soil moisture retrieval, and the low importance of the DEM (Abowarda et al.
710 2021; Karthikeyan and Mishra 2021). Overall, it is suggested that utilizing all selected input
711 variables in the downscaling model would be necessary to obtain the best downscaling
712 accuracy. Moreover, landcover type was not included here as an option due to challenges in
713 including categorical information in machine learning models. However, given the strong
714 relationship in backscatter response to different landcover types and their associated land
715 surface conditions, this could also be an important variable for use in future investigations.

716 **5. Conclusion**

717 This study presented a new strategy for downscaling the 36 km SMAP radiometer soil
718 moisture product to 1 km spatial resolution. A random forest model using 1 km resolution
719 remotely sensed backscatter, together with 1 km resolution vegetation characteristics,
720 topography and soil properties, was used to downscale 36 km resolution passive microwave
721 satellite soil moisture, based on training to focus areas with 1 km resolution soil moisture. The
722 model was trained using data acquired pre-launch of SMAP, and evaluated with post-launch of
723 SMAP airborne and field soil moisture data. Soil moisture from focus areas at 1 km spatial

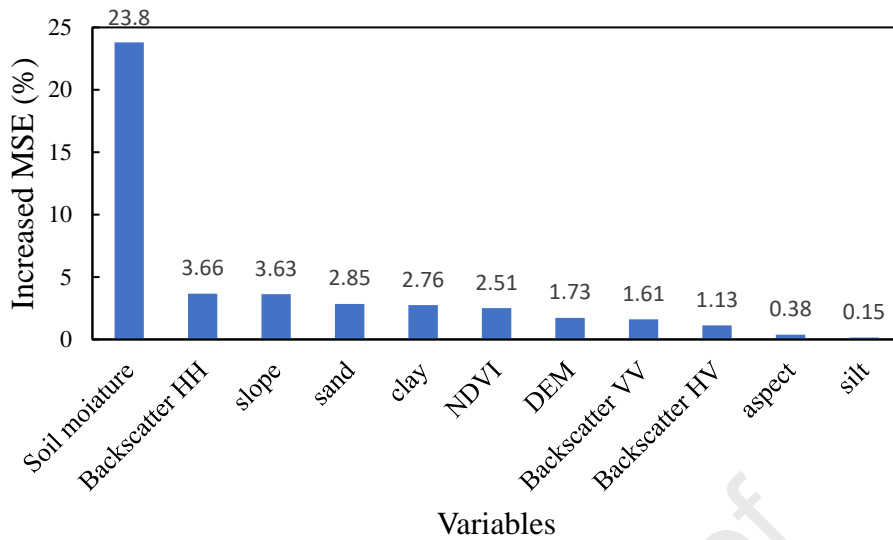


Fig. 13. Importance of input variables of the random forest model to the downscaled SMAP soil moisture calculated through increased mean square error (*MSE*) in percentage, including soil moisture, σ_{vv} , σ_{hh} , σ_{xpol} , NDVI, DEM, slope, aspect and soil texture (clay, silt and sand).

724 resolution were utilized to train the random forest algorithm, rather than the more traditional
 725 approach of using the SMAP 36 km soil moisture. The SMAP downscaled soil moisture
 726 product from the proposed random forest downscaling algorithm was then validated using post-
 727 launch airborne retrieved soil moisture observations and the ground soil moisture
 728 measurements from multiple points. This study was performed considering different soil
 729 characteristics and land cover conditions, including both grasslands and a variety of crops.

730 Based on the validation results, the downscaled SMAP soil moisture demonstrated an
 731 excellent agreement with the airborne soil moisture observations over the flight area of
 732 SMAPEX-4 and SMAPEX-5. The statistical results between the downscaled SMAP and
 733 airborne PLMR retrieved soil moisture in terms of *R*, bias and *ubRMSE* were 0.97, 0.016 m³.m⁻³
 734 ³ and 0.048 m³.m⁻³, respectively. Overall, compared to the original passive SMAP soil moisture
 735 product applied as a uniform field, the proposed downscaling random forest algorithm showed
 736 the ability to improve the *ubRMSE* of downscaled SMAP soil moisture from 0.121 m³.m⁻³ (Fig.

737 5) to $0.048 \text{ m}^3.\text{m}^{-3}$ (Fig. 6), when considering the PLMR soil moisture as a reference, being
738 close to the SMAP soil moisture accuracy requirement. The results of this study show that the
739 proposed random forest downscaling algorithm has the ability to be applied regionally by
740 training to a few local pixels at 1 km in order to downscale the coarse resolution microwave
741 soil moisture, and that training in one location (SMAPVEX-12) could be applied to another
742 location (SMAPEX). Moreover, the statistics between the downscaled SMAP and ground soil
743 moisture measurements over the SMAPEX focus areas achieved 0.79, $-0.04 \text{ m}^3.\text{m}^{-3}$ and 0.066
744 $\text{m}^3.\text{m}^{-3}$ in terms of R , bias and $ubRMSE$, respectively. Additionally, the downscaled SMAP soil
745 moisture observations satisfactorily captured the spatial and temporal heterogeneity relative to
746 ground and airborne soil moisture observations.

747 In order to investigate the importance of using data at fine spatial resolution to train the
748 random forest algorithm, as was conducted for this research, the results were compared with
749 those from the strategy of utilizing the average from a 36 km grid cell. In general, the statistical
750 metrics showed a $0.04 \text{ m}^3.\text{m}^{-3}$ improvement in terms of $ubRMSE$ downscaling accuracy by
751 using the higher spatial resolution training data, when evaluated with airborne retrieved soil
752 moisture.

753 An investigation on the importance of the input variables in the random forest algorithm
754 revealed that the best downscaling accuracy was achieved through contribution of all the input
755 variables tested. Overall, the assessment showed that the variable importance in the random
756 forest downscaling approach utilized in this study was in the following order: horizontal
757 backscatter (σ_{hh}), slope, sand, clay, NDVI, DEM, vertical backscatter (σ_{vv}), cross-polarized
758 backscatter (σ_{hv}), aspect and silt. However, the use of a landcover map should also be
759 considered in future studies.

760 **Acknowledgments**

761 The SMAPEX field campaigns and related research development have been funded by the
 762 Australian Research Council Discovery (DP0984586 and DP140100572) and Australian
 763 Research Council Linkage Infrastructure Equipment and Facilities grants (LE0882509 and
 764 LE0453434). A contribution to this work was made at the Jet Propulsion Laboratory, California
 765 Institute of Technology under a contract with the National Aeronautics and Space
 766 Administration.

767 References

- 768 Abbaszadeh, P., Moradkhani, H., & Zhan, X. (2019). Downscaling SMAP Radiometer Soil
 769 Moisture Over the CONUS Using an Ensemble Learning Method. *Water Resources Research*, *55*, 324-
 770 344
- 771 Abowarda, A.S., Bai, L., Zhang, C., Long, D., Li, X., Huang, Q., & Sun, Z. (2021). Generating
 772 surface soil moisture at 30 m spatial resolution using both data fusion and machine learning toward
 773 better water resources management at the field scale. *Remote Sensing of Environment*, *255*, 112301
- 774 Amit, Y., & Geman, D. (1997). Shape quantization and recognition with randomized trees. *Neural*
 775 *Comput.*, *9*, 1545–1588
- 776 Barre, H.M.J.P., Duesmann, B., & Kerr, Y.H. (2008). SMOS: The Mission and the System. *IEEE*
 777 *Transactions on Geoscience and Remote Sensing*, *46*, 587-593
- 778 Bindlish, R., O'Neill, P., Njoku, E., Jackson, T., Colliander, A., Chen, F., Burgin, M., Dunbar, S.,
 779 Piepmeier, J., Yueh, S., Entekhabi, D., Cosh, M., Caldwell, T., Walker, J., Wu, X., Berg, A.,
 780 Rowlandson, T., Pacheco, A., & Kerr, Y. (2016). Assessment of the SMAP Passive Soil Moisture
 781 Product. *IEEE Transactions on Geoscience and Remote Sensing*, *54*, 1-14
- 782 Breiman, L. (1996). Bagging predictors. *Machine Learning*, *24*, 123-140
- 783 Breiman, L. (2001). Random Forests. *Machine Learning*, *45*, 5-32
- 784 Bullock, P., Berg, A., & Wiseman, G. (2014). SMAPVEX12 Core-Based Soil Texture Data,
 785 Version 1. *NASA National Snow and Ice Data Center Distributed Active Archive Center*
- 786 Chan, S., Bindlish, R., O'Neill, P., Njoku, E., Jackson, T., Colliander, A., Chen, F., Burgin, M.,
 787 Dunbar, S., Piepmeier, J., Yueh, S., Entekhabi, D., Cosh, M., Caldwell, T., Walker, J., Wu, X., Berg,
 788 A., Rowlandson, T., Pacheco, A., & Kerr, Y. (2016). Assessment of the SMAP Passive Soil Moisture
 789 Product. *IEEE Transactions on Geoscience and Remote Sensing*, *54*, 1-14
- 790 Colliander, A. (2014). SMAPVEX12 PALS Backscatter Data, Version 1 [Data Set]. In. Boulder,
 791 Colorado USA.: NASA National Snow and Ice Data Center Distributed Active Archive Center.
- 792 Colliander, A. (2017). SMAPVEX12 PALS Soil Moisture Data, Version 1 [Data Set]. In. Boulder,
 793 Colorado USA.: NASA National Snow and Ice Data Center Distributed Active Archive Center.
- 794 Colliander, A., Fisher, J.B., Halverson, G., Merlin, O., Misra, S., Bindlish, R., Jackson, T.J., &
 795 Yueh, S. (2017a). Spatial Downscaling of SMAP Soil Moisture Using MODIS Land Surface
 796 Temperature and NDVI During SMAPVEX15. *IEEE Geoscience and Remote Sensing Letters*, *14*,
 797 2107-2111
- 798 Colliander, A., Jackson, T.J., Bindlish, R., Chan, S., Das, N., Kim, S.B., Cosh, M., Dunbar, R.S.,
 799 Dang, L., Pashaian, L., Asanuma, J., Aida, K., Berg, A., Rowlandson, T., Bosch, D., Caldwell, T.,
 800 Caylor, K., Goodrich, D., Aljassar, H.K., & Yueh, S. (2017b). Validation of SMAP surface soil moisture
 801 products with core validation sites. *Remote Sensing of Environment*, *191*, 215-231
- 802 Colliander, A., Njoku, E.G., Jackson, T.J., Chazanoff, S., McNairn, H., Powers, J., & Cosh, M.H.
 803 (2016). Retrieving soil moisture for non-forested areas using PALS radiometer measurements in
 804 SMAPVEX12 field campaign. *Remote Sensing of Environment*, *184*, 86-100

- 805 Crow, W.T., Berg, A.A., Cosh, M.H., Loew, A., Mohanty, B.P., Panciera, R., de Rosnay, P., Ryu,
806 D., & Walker, J.P. (2012). Upscaling sparse ground-based soil moisture observations for the validation
807 of coarse-resolution satellite soil moisture products. *Reviews of Geophysics*, 50
- 808 Das, N., Entekhabi, D., & Njoku, E. (2011). An Algorithm for Merging SMAP Radiometer and
809 Radar Data for High-Resolution Soil-Moisture Retrieval. *Geoscience and Remote Sensing, IEEE*
810 *Transactions on*, 49, 1504-1512
- 811 Das, N.N., Entekhabi, D., Dunbar, R.S., Chaubell, M.J., Colliander, A., Yueh, S., Jagdhuber, T.,
812 Chen, F., Crow, W., O'Neill, P.E., Walker, J.P., Berg, A., Bosch, D.D., Caldwell, T., Cosh, M.H.,
813 Collins, C.H., Lopez-Baeza, E., & Thibeault, M. (2019). The SMAP and Copernicus Sentinel 1A/B
814 microwave active-passive high resolution surface soil moisture product. *Remote Sensing of*
815 *Environment*, 233, 111380
- 816 Entekhabi, D., G. Njoku, E., E. O'Neill, P., Kellogg, K.H., Crow, W., Edelstein, W.N., Entin, J., D.
817 Goodman, S., J. Jackson, T., Johnson, J., Kimball, J., Piepmeier, J., D. Koster, R., Martin, N.,
818 McDonald, K., Moghaddam, M., Moran, S., Reichle, R., Shi, J., & van Zyl, J. (2010). *The Soil Moisture*
819 *Active and Passive (SMAP) mission*.
- 820 Entekhabi, D., Yueh, S., O'Neill, P.E., Kellogg, K.H., Allen, A., Bindlish, R., Brown, M., Chan,
821 S., Colliander, A., Crow, W.T., Das, N., De Lannoy, G., Dunbar, R.S., Edelstein, W.N., Entin, J.K.,
822 Escobar, V., Goodman, S.D., Jackson, T.J., Jai, B., Johnson, J., Kim, E., Kim, S., Kimball, J., Koster,
823 R.D., Leon, A., McDonald, K.C., Moghaddam, M., Mohammed, P., Moran, S., Njoku, E.G., Piepmeier,
824 J.R., Reichle, R., Rogez, F., Shi, J.C., Spencer, M.W., Thurman, S.W., Tsang, L., Van Zyl, J., Weiss,
825 B., & West, R. (2014). SMAP Handbook–Soil Moisture Active Passive: Mapping Soil Moisture and
826 Freeze/Thaw from Space
- 827 Fang, B., & Lakshmi, V. (2014). AMSR-E Soil Moisture Disaggregation Using MODIS and
828 NLDAS Data. *Remote Sensing of the Terrestrial Water Cycle*, 277-304
- 829 Fang, K., & Shen, C. (2020). Near-Real-Time Forecast of Satellite-Based Soil Moisture Using Long
830 Short-Term Memory with an Adaptive Data Integration Kernel. *Journal of Hydrometeorology*, 21, 399-
831 413
- 832 Gao, Y., Colliander, A., Burgin, M.S., Walker, J.P., Dinnat, E., Chae, C., Cosh, M.H., Caldwell,
833 T.G., Berg, A., Martinez-Fernandez, J., Seyfried, M., Starks, P.J., Bosch, D.D., McNairn, H., Su, Z., &
834 van der Velde, R. (2022). Multi-frequency radiometer-based soil moisture retrieval and algorithm
835 parameterization using in situ sites. *Remote Sensing of Environment*, 279, 113113
- 836 Ghafari, E., Walker, J.P., Das, N.N., Davary, K., Faridhosseini, A., Wu, X., & Zhu, L. (2020). On
837 the impact of C-band in place of L-band radar for SMAP downscaling. *Remote Sensing of Environment*,
838 251, 112111
- 839 Hastie, T., Tibshirani, R., & Friedman, J. (2009). *The Elements of Statistical Learning: Data*
840 *Mining, Inference, and Prediction, Second Edition (Springer Series in Statistics)*.
- 841 He, X., Chaney, N.W., Schleiss, M., & Sheffield, J. (2016). Spatial downscaling of precipitation
842 using adaptable random forests. *Water Resources Research*, 52, 8217-8237
- 843 Hu, F., Wei, Z., Zhang, W., Dorjee, D., & Meng, L. (2020). A spatial downscaling method for
844 SMAP soil moisture through visible and shortwave-infrared remote sensing data. *Journal of Hydrology*,
845 590, 125360
- 846 Karthikeyan, L., & Mishra, A.K. (2021). Multi-layer high-resolution soil moisture estimation using
847 machine learning over the United States. *Remote Sensing of Environment*, 266, 112706
- 848 Kerr, Y.H., Waldteufel, P., Richaume, P., Wigneron, J.P., Ferrazzoli, P., Mahmoodi, A., Bitar,
849 A.A., Cabot, F., Gruhier, C., Juglea, S.E., Leroux, D., Mialon, A., & Delwart, S. (2012). The SMOS
850 Soil Moisture Retrieval Algorithm. *IEEE Transactions on Geoscience and Remote Sensing*, 50, 1384-
851 1403
- 852 Kim, Y., & Zyl, J.J.v. (2009). A Time-Series Approach to Estimate Soil Moisture Using
853 Polarimetric Radar Data. *IEEE Transactions on Geoscience and Remote Sensing*, 47, 2519-2527
- 854 Lei, F., Senyurek, V., Kurum, M., Gurbuz, A., Boyd, D., Moorhead, R., Crow, W., & Eroglu, O.
855 (2022). Quasi-global machine learning-based soil moisture estimates at high spatio-temporal scales
856 using CYGNSS and SMAP observations. *Remote Sensing of Environment*, 276, 113041
- 857 Long, D., Bai, L., Yan, L., Zhang, C., Yang, W., Lei, H., Quan, J., Meng, X., & Shi, C. (2019).
858 Generation of spatially complete and daily continuous surface soil moisture of high spatial resolution.
859 *Remote Sensing of Environment*, 233, 111364

- 860 Mao, H., Kathuria, D., Duffield, N., & Mohanty, B.P. (2019). Gap Filling of High-Resolution Soil
861 Moisture for SMAP/Sentinel-1: A Two-Layer Machine Learning-Based Framework. *Water Resources*
862 *Research*, 55, 6986-7009
- 863 Mao, T., Shangguan, W., Li, Q., Li, L., Zhang, Y., Huang, F., Li, J., Liu, W., & Zhang, R. (2022).
864 A Spatial Downscaling Method for Remote Sensing Soil Moisture Based on Random Forest
865 Considering Soil Moisture Memory and Mass Conservation. *Remote Sensing*, 14, 3858
- 866 Mascaro, G., Vivoni, E., & Deidda, R. (2011). Soil moisture downscaling across climate regions
867 and its emergent properties. *J. Geophys. Res*, 116
- 868 McNairn, H., Jackson, T.J., Wiseman, G., Bélair, S., Berg, A., Bullock, P., Colliander, A., Cosh,
869 M.H., Kim, S.B., Magagi, R., Moghaddam, M., Njoku, E.G., Adams, J.R., Homayouni, S., Ojo, E.R.,
870 Rowlandson, T.L., Shang, J., Goïta, K., & Hosseini, M. (2015). The Soil Moisture Active Passive
871 Validation Experiment 2012 (SMAPVEX12): Prelaunch Calibration and Validation of the SMAP Soil
872 Moisture Algorithms. *IEEE Transactions on Geoscience and Remote Sensing*, 53, 2784-2801
- 873 Merlin, O., Rudiger, C., Bitar, A.A., Richaume, P., Walker, J.P., & Kerr, Y.H. (2012).
874 Disaggregation of SMOS Soil Moisture in Southeastern Australia. *IEEE Transactions on Geoscience*
875 *and Remote Sensing*, 50, 1556-1571
- 876 Merlin, O., Walker, J., Panciera, R., Young, R., Kalma, J., & Kim, E. (2007). Soil Moisture
877 Measurement in Heterogeneous Terrain. *MODSIM 2007 International Congress on Modelling and*
878 *Simulation*
- 879 Merlin, O., Walker, J.P., Chehbouni, A., & Kerr, Y. (2008). Towards deterministic downscaling of
880 SMOS soil moisture using MODIS derived soil evaporative efficiency. *Remote Sensing of Environment*,
881 112, 3935-3946
- 882 Monerris, A., Walker, J., Panciera, R., Jackson, T., Gray, D., Yardley, H., & Ryu, D. (2011). *The*
883 *Third Soil Moisture Active Passive Experiment*.
- 884 Narayan, U., Lakshmi, V., & Jackson, T.J. (2006). High-resolution change estimation of soil
885 moisture using L-band radiometer and Radar observations made during the SMEX02 experiments.
886 *IEEE Transactions on Geoscience and Remote Sensing*, 44, 1545-1554
- 887 O'Neill, P.E., Chan, S., Njoku, E.G., Jackson, T., Bindlish, R., & Chaubell, J. (2021). SMAP L3
888 Radiometer Global Daily 36 km EASE-Grid Soil Moisture, Version 8. *Boulder, Colorado USA. NASA*
889 *National Snow and Ice Data Center Distributed Active Archive Center*
- 890 O, S., & Orth, R. (2021). Global soil moisture data derived through machine learning trained with
891 in-situ measurements. *Scientific Data*, 8, 170
- 892 Panciera, R., Walker, J.P., Jackson, T.J., Gray, D.A., Tanase, M.A., Ryu, D., Monerris, A., Yardley,
893 H., Rüdiger, C., Wu, X., Gao, Y., & Hacker, J.M. (2014). The Soil Moisture Active Passive Experiments
894 (SMAPEx): Toward Soil Moisture Retrieval From the SMAP Mission. *IEEE Transactions on*
895 *Geoscience and Remote Sensing*, 52, 490-507
- 896 Piles, M., Camps, A., Vall-llossera, M., Corbella, I., Panciera, R., Rüdiger, C., Kerr, Y., & Walker,
897 J. (2011). Downscaling SMOS-derived soil moisture using MODIS Visible/Infrared data. *Geoscience*
898 *and Remote Sensing, IEEE Transactions on*, 49, 3156-3166
- 899 Rao, P., Wang, Y., Wang, F., Liu, Y., Wang, X., & Wang, Z. (2022). Daily soil moisture mapping
900 at 1 km resolution based on SMAP data for desertification areas in northern China. *Earth Syst.*
901 *Sci. Data*, 14, 3053-3073
- 902 Sabaghy, S., Walker, J.P., Renzullo, L.J., Akbar, R., Chan, S., Chaubell, J., Das, N., Dunbar, R.S.,
903 Entekhabi, D., Gevaert, A., Jackson, T.J., Loew, A., Merlin, O., Moghaddam, M., Peng, J., Peng, J.,
904 Piepmeier, J., Rüdiger, C., Stefan, V., Wu, X., Ye, N., & Yueh, S. (2020). Comprehensive analysis of
905 alternative downscaled soil moisture products. *Remote Sensing of Environment*, 239, 111586
- 906 Sabaghy, S., Walker, J.P., Renzullo, L.J., & Jackson, T.J. (2018). Spatially enhanced passive
907 microwave derived soil moisture: Capabilities and opportunities. *Remote Sensing of Environment*, 209,
908 551-580
- 909 Schmugge, T., O'Neill, P.E., & Wang, J.R. (1986). Passive microwave soil moisture research. *IEEE*
910 *Transactions on Geoscience and Remote Sensing*, 12-22
- 911 Senanayake, I.P., Yeo, I.Y., Walker, J.P., & Willgoose, G.R. (2021). Estimating catchment scale
912 soil moisture at a high spatial resolution: Integrating remote sensing and machine learning. *Science of*
913 *The Total Environment*, 776, 145924

- 914 Seneviratne, S.I., Corti, T., Davin, E.L., Hirschi, M., Jaeger, E.B., Lehner, I., Orlowsky, B., &
 915 Teuling, A.J. (2010). Investigating soil moisture–climate interactions in a changing climate: A review.
 916 *Earth-Science Reviews*, 99, 125-161
- 917 Srivastava, P.K., Han, D., Ramirez, M.R., & Islam, T. (2013). Machine Learning Techniques for
 918 Downscaling SMOS Satellite Soil Moisture Using MODIS Land Surface Temperature for Hydrological
 919 Application. *Water Resources Management*, 27, 3127-3144
- 920 Wilson, D.J., Western, A.W., & Grayson, R.B. (2005). A terrain and data-based method for
 921 generating the spatial distribution of soil moisture. *Advances in Water Resources*, 28, 43-54
- 922 Wu, X., Walker, J., Rüdiger, C., Panciera, R., & Gao, Y. (2016). Intercomparison of Alternate Soil
 923 Moisture Downscaling Algorithms Using Active-Passive Microwave Observations. *IEEE Geoscience
 924 and Remote Sensing Letters*, PP, 1-5
- 925 Wu, X., Walker, J.P., Rüdiger, C., Panciera, R., & Gray, D.A. (2015). Simulation of the SMAP
 926 Data Stream From SMAPEX Field Campaigns in Australia. *IEEE Transactions on Geoscience and
 927 Remote Sensing*, 53, 1921-1934
- 928 Ye, N., Walker, J.P., & Rüdiger, C. (2015). A Cumulative Distribution Function Method for
 929 Normalizing Variable-Angle Microwave Observations. *IEEE Transactions on Geoscience and Remote
 930 Sensing*, 53, 3906-3916
- 931 Ye, N., Walker, J.P., Wu, X., Jeu, R.d., Gao, Y., Jackson, T.J., Jonard, F., Kim, E., Merlin, O.,
 932 Pauwels, V.R.N., Renzullo, L.J., Rüdiger, C., Sabaghy, S., Hebel, C.v., Yueh, S.H., & Zhu, L. (2020).
 933 The Soil Moisture Active Passive Experiments: Validation of the SMAP Products in Australia. *IEEE
 934 Transactions on Geoscience and Remote Sensing*, 1-18
- 935 Zhao, W., Sánchez, N., Lu, H., & Li, A. (2018). A spatial downscaling approach for the SMAP
 936 passive surface soil moisture product using random forest regression. *Journal of Hydrology*, 563, 1009-
 937 1024
- 938 Zhu, L., Walker, J.P., & Shen, X. (2020). Stochastic ensemble methods for multi-SAR-mission soil
 939 moisture retrieval. *Remote Sensing of Environment*, 251, 112099
- 940 Zhu, L., Walker, J.P., Ye, N., Rüdiger, C., Hacker, J.M., Panciera, R., Tanase, M.A., Wu, X., Gray,
 941 D.A., Stacy, N., Goh, A., Yardley, H., & Mead, J. (2018). The Polarimetric L-Band Imaging Synthetic
 942 Aperture Radar (PLIS): Description, Calibration, and Cross-Validation. *IEEE Journal of Selected
 943 Topics in Applied Earth Observations and Remote Sensing*, 11, 4513-4525
- 944 Zhu, L., Webb, G.I., Yebra, M., Scortechini, G., Miller, L., & Petitjean, F. (2021). Live fuel
 945 moisture content estimation from MODIS: A deep learning approach. *ISPRS Journal of
 946 Photogrammetry and Remote Sensing*, 179, 81-91

947

Declaration of interests

The authors declare that they have no known competing financial interests or personal relationships that could have appeared to influence the work reported in this paper.

The authors declare the following financial interests/personal relationships which may be considered as potential competing interests:

Journal Pre-proof